GAS TURBINE LABORATORY
DEPARTMENT OF AERONAUTICS AND ASTRONAUTICS
MASSACHUSETTS INSTITUTE OF TECHNOLOGY
CAMBRIDGE, MA 02139

FINAL TECHNICAL REPORT FOR

GRANT NO. NAG 3-9

ENTITLED

RESEARCH APPLIED TO TRANSONIC COMPRESSORS IN NUMERICAL FLUID MECHANICS OF INVISCID FLOW AND VISCOUS FLOW

SUBMITTED TO THE

NASA LEWIS RESEARCH CENTER
CLEVELAND, OH 44135

ATTN: R.V. CHIMA, TECHNICAL OFFICER

Period of Investigation: December 1, 1979 - November 30, 1984

Principal Investigator: W.T. Thompkins, Jr., Associate Professor
Department of Aeronautics and Astronautics

February 1985

SUMMARY

Research work on NASA Grant NAG 3-9 concentrated on development of numerical methods for the Euler equations and on development of analysis methods for these equations. Results of this work have been published as journal articles, AIAA papers, student theses, and MIT internal reports. The most important results were a streamtube Euler solver which combines high accuracy and good convergence rates with capabilities for inverse or direct mode solution modes and an analysis technique for finite difference models of hyperbolic partial difference equations.

Two graduate students, Robert Bush and Michael Giles, were partially supported by this grant. Robert Bush received his S.M. degree in February 1981 and his Ph.D. degree in September 1983. Michael Giles received his S.M. degree in September 1982. Michael was also supported for a summer visit to ICASE in 1983.

TECHNICAL SUMMARY

The earliest work on this grant was computational work on approximate factorization (AF) methods for Euler and Navier-Stokes equations and was performed by Robert Bush. The major new result from his work was recognition that the optimum time step size for AF methods was not necessarily the largest stable time step. This result has now been substantiated by other analytical and computational results. A Jour. of Comp. Physics paper [1] and an S.M. thesis [2] were published during this phase. A copy of Reference 1 is included in the Appendix.

The next phase of effort on the grant concentrated on a new analysis method applied to finite difference methods for hyperbolic equations, and was performed by Michael Giles. This work developed group velocity concepts for finite difference equations to explain spurious traveling wave solutions, dissipation and stability of inflow/outflow boundary conditions, and convergence rates. During this phase, a Jour. of Comp. Physics paper [3], an IMACS symposium paper [4], an ICASE contractor report [5] and a S.M. thesis [6] were published. References 3, 4, and 5 are included in the Appendix.

The last phase of the grant work examined new solution methods for the Euler equations and was also conducted by Michael Giles. Major results from this work were a box-type method for the quasi-one-dimensional Euler equations, and a streamtube method for the two-dimensional Euler equations. Both methods are substantially faster than other comparable solution schemes. An AIAA paper [7] was published on the streamtube method, and an internal MIT report [8] was published on the box method. References 7 and 8 are included in the Appendix.

References

1. Thompkins, W.T. and Bush, R.H., "Boundary Treatments for Implicit Solutions to Euler and Navier-Stokes Equations," J.Comp.Phys., Vol. 48, No. 2, November 1982.

2. Bush, R.H., "Time Accurate Flow Solutions of the Thin Shear Layer Equations," S.M. Thesis, Dept. of Aero and Astro, February 1981.

3. Giles, M.B., Thompkins, W.T., "Propagation, Stability and Convergence of Wavelike Solutions of Finite Difference Equations with Variable Coefficients," accepted for publication in J.Comp.Phys.

4. Giles, M.B., Thompkins, W.T., "Internal Reflection Due to a Nonuniform Grid," Proceedings of 5th IMACS International Symposium on Computer Methods for Partial Differential Equations, Lehigh Univ., June 19, 1984.

5. Giles, M., "Eigenmode Analysis of Unsteady One-Dimensional Euler Equations," NASA Contractor Report, ICASE, August 1983

6. Giles, M., Thompkins, W.T., "Asymptotic Analysis of Numerical Wave Propagation in Finite Difference Equations," GT&PDL Report 171, March 1983.

7. Drela, M., Giles, M., Thompkins, W.T., "Conservative Streamtube Solution of Steady-State Euler Equations," AIAA Paper 84-1643.

8. Giles, M., "Solution of 1-D Euler Equations Using A Box Method," CFDL-TR-84-1, February 1984.

Reprinted from JOURNAL OF COMPUTATIONAL PHYSICS
All Rights Reserved by Academic Press, New York and London

Vol. 48, No. 2, November 1982
Printed in Belgium

Note

Boundary Treatments for Implicit Solutions to Euler and Navier–Stokes Equations

INTRODUCTION

Implicit time marching schemes like those of Beam and Warning [1], Briley and MacDonald [2], and MacCormack (1980) [3] generally have not been as robust as would be expected from a stability analysis for the pure initial value problem. Recently, Yee *et al.* [4] illustrated that a more general stability analysis, which includes the effect of boundary conditions, may explain some of the seemingly anomalous behavior of these schemes. The major theoretical basis for this type of modal stability was established in a series of papers by Kreiss [5, 6], Osher [7, 8], and Gustafsson *et al.* [9].

Yee as well as Gustafsson and Oliger [10] considered the effect of inflow–outflow boundary condition formulations on the stability of a class of numerical schemes to solve the Euler equations in one space dimension. The characteristic feature of a subsonic inflow–outflow boundary is that a priori boundary values may be specified for only some problem variables, while remaining boundary values must be determined as part of the solution process. Yee demonstrated a rather large disparity in stability bounds between the use of explicit or implicit extrapolation procedures and in general demonstrated that implicit extrapolation procedures had the least restrictive stability bounds. The intent here is to explore computationally the implication of this work for several two-dimensional Euler and Navier–Stokes simulations.

NUMERICAL PROCEDURES

The two-dimensional Navier–Stokes equations may be written in vector form as [1]

$$\frac{\partial U}{\partial t}+\frac{\partial E}{\partial x}+\frac{\partial F}{\partial y}=\frac{\partial R}{\partial x}+\frac{\partial S}{\partial y}. \tag{1}$$

The strong conservation law form may be retained under a general coordinate mapping as illustrated in Viviand [11]. All computations to be described were conducted in a mapped computational domain but for simplicity numerical and

0021-9991/82/110302-10$02.00/0

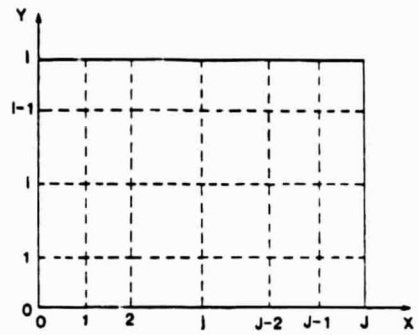

FIG. 1. Grid numbering schene for boundary condition formulation.

boundary condition procedures will be described in the simple two-dimensional geometry shown in Fig. 1.

A 1979 paper by Beam and Warning [12] outlined a solution scheme for systems of equations of form (1) which included most numerical schemes for which the modal boundary condition analysis has been conducted. This scheme uses the well-developed methods for ordinary differential equations as a guide to developing numerical methods for partial differential equations. The scheme presented combines linear multistep methods, local linearization, approximate factorization, and one leg methods. The shceme, a generalization of the scheme presented in [1], solves for a variable $\rho(E)\, u$ which is equivalent to Δu^n in the class of schemes represented by the earlier paper. The earlier scheme is somewhat easier to understand as Δu^n is just the change in the solution from time level n to level $n+1$, while $\rho(E)\, u$ is a more general time differencing formula.

The solution schemes chosen are implemented as

$$(I + L_y^n)\,\Delta u^* = RHS^n, \tag{2}$$

$$(I + L_x^n)\,\Delta U^n = \Delta U^*, \tag{3}$$

$$U^{n+1} = U^n + \Delta U^n, \tag{4}$$

where RHS^n is very nearly the finite difference approximation to the steady state equations, and L_x and L_y are linearized difference operators representing a particular time and spatial differencing scheme.

Full details of these operators are contained in [1]. If the spatial differencing is taken to be centered, the computational form of either Eq. (2) or (3) appears at each interior point as

$$A_i^n \Delta U_{i-1}^n + B_i^n \Delta U_i^n + C_i^n \Delta U_{i+1}^n = D_i^n, \tag{5}$$

where A_i, B_i, and C_i are 4×4 matrices known at time level n, D_i is the right-hand side vector at node point i known at time level n, and ΔU_i^n is the unknown vector at

node point i. The boundary points will be assumed to involve only the nearest two points in the x direction.

$$A_0^n \Delta U_0 + B_0^n \Delta U_1 + C_0^n \Delta U_2 = D_0^n. \tag{6}$$

The restriction to extrapolation along grid lines (actually transformed grid lines), is necessary to maintain the block tridiagonal form and avoids possible instabilities due to skewed extrapolation, see [13].

The full matrix equation will reduce to tridiagonal form if the first and nth equations are substituted into the second and the $(n-i)$th equations, for example,

$$B_1' = B_1 - A_1 A_0^{-1} B_0. \tag{7}$$

Boundary Treatments

Inflow–outflow Boundary

The finite difference algorithms studied usually require more boundary values than are required for the partial differential equations which they simulate. These extra numerical boundary conditions cannot be set arbitrarily and are usually determined through an extrapolation procedure. These extrapolation procedures may either be explicit, that is boundary values needed at a new time are determined uniquely from the old time level solution, or implicit, that is, the boundary values are determined as part of the new time level solution. The analytical boundary conditions or the extrapolation quantities are usually not conservation variables but primitive variables, and a local linearization is usually required as part of defining the extrapolation procedure.

Consider, for example, an implicit subsonic outflow boundary at which the local static pressure is specified as a boundary condition and all other variables are to be determined by extrapolation. Figure 1 shows a typical computational grid and defines the subscripts used.

$$P_{i,j}^{n+1} = P_{i,j}^n \qquad \text{given,} \tag{8}$$

$$\begin{pmatrix} \rho \\ \rho u \\ \rho v \end{pmatrix}_{i,j}^{n+1} = 2\begin{pmatrix} \rho \\ \rho u \\ \rho v \end{pmatrix}_{i,j-1}^{n+1} - \begin{pmatrix} \rho \\ \rho u \\ \rho v \end{pmatrix}_{i,j-2}^{n+1} \qquad \text{implicit space extrapolation.} \tag{9}$$

In order to complete the boundary formulation, all equations must be expressed in delta form and in terms of conservation variables. For the total internal energy this may be done through its definition

$$E_t = P/(\gamma - 1) + \tfrac{1}{2}(\rho u)^2/\rho + (v)^2/\rho. \tag{10}$$

Since the relations between conservation variables are nonlinear, some linearization

step will be necessary before the boundary condition formulation may be used. We choose to introduce our linearization step here as

$$\Delta E_t = (E_t^{n+1} - E_t^n) = (1/(\gamma - 1))\,\Delta P - \tfrac{1}{2}(u^2 + v^2)^n\,\Delta\rho + u^n\Delta(\rho u) + v^n\Delta(\rho v) + (\Delta u\Delta v, \Delta u^2, \Delta v^2, \Delta\rho\Delta u, \Delta\rho\Delta v). \tag{11}$$

If terms of order $\Delta u\Delta v$ are neglected, the error is equivalent to the linearization error of the interior point scheme. We may express the transformation from boundary variables to conservation variables as

$$U_{i,j} = \begin{pmatrix} \Delta\rho \\ \Delta\rho u \\ \Delta\rho v \\ \Delta E_t \end{pmatrix}_{i,j} = \begin{pmatrix} 1 & 0 & 0 & 0 \\ 0 & 1 & 0 & 0 \\ 0 & 0 & 1 & 0 \\ -\tfrac{1}{2}(u^2 + v^2)^n & u^n & v^n & 1/(\gamma - 1) \end{pmatrix} \begin{pmatrix} \Delta\rho \\ \Delta\rho u \\ \Delta\rho v \\ \Delta P \end{pmatrix} = N_{i,j}\Delta W_{i,j} \tag{12}$$

we shall in general denote transformation from conservative to primitive variables as

$$\Delta W_{i,j} = T_{i,j}\Delta U_{i,j}. \tag{13}$$

The extrapolation conditions for $W_{i,j}$ are

$$\Delta W_{i,J} = \begin{pmatrix} \Delta\rho \\ \Delta\rho u \\ \Delta\rho v \\ \Delta P \end{pmatrix}_{i,J} = \begin{pmatrix} 2 & 0 & 0 & 0 \\ 0 & 2 & 0 & 0 \\ 0 & 0 & 2 & 0 \\ 0 & 0 & 0 & 0 \end{pmatrix} \begin{pmatrix} \Delta\rho \\ \Delta\rho u \\ \Delta\rho v \\ \Delta P \end{pmatrix}_{i,J-1} + \begin{pmatrix} -1 & 0 & 0 & 0 \\ 0 & -1 & 0 & 0 \\ 0 & 0 & -1 & 0 \\ 0 & 0 & 0 & 0 \end{pmatrix} \begin{pmatrix} \Delta\rho \\ \Delta\rho u \\ \Delta\rho v \\ \Delta P \end{pmatrix}_{i,J-2} \tag{14}$$

or

$$\Delta W_{i,J} = P_{J-1}W_{i,J-1} + P_{J-2}W_{i,J-2}. \tag{15}$$

The final equations relating the boundary conservation variables and the interior conservation variables are

$$\Delta U_{i,J} = N_{i,J}^n(P_{J-1}T_{i,J-1}^n\Delta U_{i,J-1} + P_{J-2}T_{i,J-1}^n\Delta U_{i,J-2}) \tag{15}$$

or

$$\Delta U_{i,J}G_{i,J-1}^n\Delta U_{i,J-1} + H_{i,J-2}^n\Delta U_{i,J-2}. \tag{17}$$

With the definition of P_{J-1} and P_{J-2} given in Eq. (15), $T_{i,J-1}$ and $T_{i,J-2}$ are identity matrices.

An explicit outflow boundary treatment was constructed using

$$P^{n+1} = P^n, \qquad \text{given},$$

$$\begin{pmatrix} \rho \\ \rho u \\ \rho v \end{pmatrix}_{I,J}^{n+1} = \begin{pmatrix} \rho \\ \rho u \\ \rho v \end{pmatrix}_{I,J-1}^{n}, \tag{18}$$

and setting $G_{I,J-1} = H_{I,J-2} = 0$.

In forming Eq. (9), we choose to extrapolate the local momentum flux rather than a specific primitive or characteristic variable; choice of other extrapolation variables would alter only the transformation matrix $T_{i,j}$. Extrapolation of the momentum flux is somewhat arbitrary, but its choice did not affect the accuracy of the computational results to be presented.

Solid Wall Boundary Procedures

The boundary treatment procedure illustrated for inflow–outflow boundary are easily extended to cover solid walls in either inviscid or viscous flow situations. Here

$$\Delta U_{0,J} = \begin{pmatrix} \Delta\rho \\ \Delta\rho u \\ \Delta\rho v \\ \Delta E_t \end{pmatrix} = \begin{pmatrix} \gamma/T & \rho/T & 0 & 0 \\ \gamma u/T & \rho u/T & 0 & 0 \\ \gamma v/T & \rho v/T & 0 & Sq \\ \dfrac{1}{\gamma-1} + \dfrac{1}{2}\dfrac{\gamma q^2}{T} & -\dfrac{1}{2}\dfrac{\rho q}{T} & \rho q & 0 \end{pmatrix} \begin{pmatrix} \Delta P \\ \Delta T \\ \Delta q \\ \Delta u \end{pmatrix} \tag{19}$$

or

$$\Delta U_{0,J} = N_{0,J}^n \Delta W_{0,J}, \tag{20}$$

where q is the velocity parallel to the wall and S is the wall slope. For the inviscid flow examples $\partial P/\partial y$, $\partial T/\partial y$, and $\partial q/\partial y$ are set equal to zero, while, for the viscous flow examples v, u, and $\partial T/\partial Y$ are set equal to zero and $\partial P/\partial y$ is equal to $4/3\mu(\partial^2/\partial y^2)(v)$. All derivatives are evaluated by one-sided finite difference formulas.

As indicated by Buggeln *et al.* [14], an ADI type procedure requires boundary conditions for the intermediate step. Usually the intermediate step was in the y direction and the boundary conditions were applied as if the intermediate results were physical quantities, that is, the boundary conditions of Eq. (19) were applied to the quantities ΔU^* of Eq. (2).

Explicit wall boundary treatments are generated by applying the primitive variable form of Eq. (19) and forcing the correction matrices to be zero.

Numerical Results

Three geometries were selected for detailed study: an inviscid supersonic diffuser with weak oblique shock, supersonic in/supersonic out; an inviscid supersonic

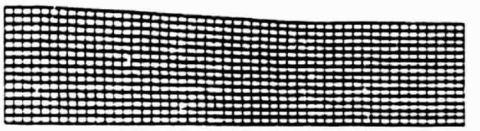

FIG. 2. Computational grid for weak shock diffuser calculations.

diffuser with a strong normal shock, supersonic in/subsonic out, and a viscous supersonic diffuser with weak oblique shock illustrating a shock-boundary layer interaction. Sketches of the geometries are shown in Figs. 2–4. Solutions for each geometry were run to steady state for a range of time step sizes. For convenience, time step sizes are reported in terms of x and y CFL numbers

$$(\mathrm{CFL}_x) = \max(\Delta t(u + c)_{i,j}/\Delta x_{i,j}), \tag{21}$$

$$(\mathrm{CFL})_y = \max(\Delta t(v + c)_{i,j}/\Delta y_{i,j}). \tag{22}$$

The time step size was uniform over each calculation which results in nonuniform CFL_x and CFL_y numbers. The maximum value of each is reported. Sample convergence history plots are shown in Fig. 5 which shows the log of the value of the point maximum steady state residual

$$\mathrm{SSR} = \partial E/\partial x - \partial R/\partial x + \partial F/\partial y - \partial S/\partial y \tag{23}$$

plotted against the iteration number. A solution was not termed stable unless the residual converged to the machine accuracy, about 1×10^{-6}. All calculations used a 32 bit floating point word size.

Each geometry calculation was run with fully explicit extrapolations, $\Delta u = 0$, and with fully implicit extrapolations; the results are summarized in Table I. The most interesting of these results are shown in Fig. 5. At a tipe step size corresponding to a CFL_x number of 15, convergence was rapid and very nearly monotonic in time. At smaller time step sizes, the convergence was slower but nearly monotonic. At a CFL_x of 45, convergence rates initially appeared to be faster than for a CFL_x of 15, but the final residual values oscillated sugnificantly about its minimum value. At a CFL_x of 90, the convergence rate was substantially slower than at a CFL_x of 15, and at larger CFL_x values the solution diverged.

The results for the strong shock diffuser can reasonably be compared to those of Yee *et al.* [4]. They reported a CFL number stability limit between 10 and 20, while

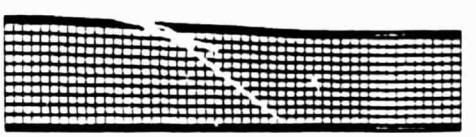

FIG. 3. Computational grid for shock-boundary layer calculations.

TABLE I

	Inviscid weak oblique shock diffuser			Inviscid strong shock diffuser			Shock boundary layer		
	CFL_x	CFL_y	Iterations to convergence	CFL_x	CFL_y	Iterations to convergence	CFL_x	CFL_y	Iterations to convergence
Explicit boundary treatments	1.5	0.6	225	1.5	0.6	3000	1.5	125	1300
	6.0	2.4	130	6.0	2.4	1200	6.0	500	unstable
	15.0	6.0	225	15.0	6.0	800	15.0	1250	unstable
	45.0	18.0	500	45.0	18.0	800	45.0	3750	unstable
	90.0	36.0	1000	90.0	36.0	1000	90.0	7500	unstable
	150.0	60.0	3000	150.0	60.0	3000	150.0	12500	unstable
Implicit boundary treatments	1.5	0.6	225	1.5	0.6	3000	1.5	125	1300
	6.0	2.4	130	6.0	2.4	950	6.0	500	400
	15.0	6.0	225	15.0	6.0	400	15.0	1250	unstable
	45.0	18.0	500	45.0	18.0	1000	45.0	3750	unstable
	90.0	36.0	1000	90.0	36.0	1500	90.0	7500	unstable
	150.0	60.0	unstable	150.0	60.0	unstable	150.0	12500	unstable
	15.0	1250	250				15.0	600	unstable

Note. Backward Euler time differencing was used for all reported calculations.

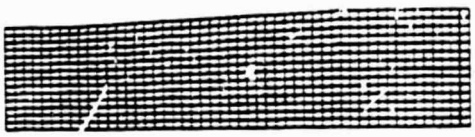

FIG. 4. Computational grid for strong shock calculations.

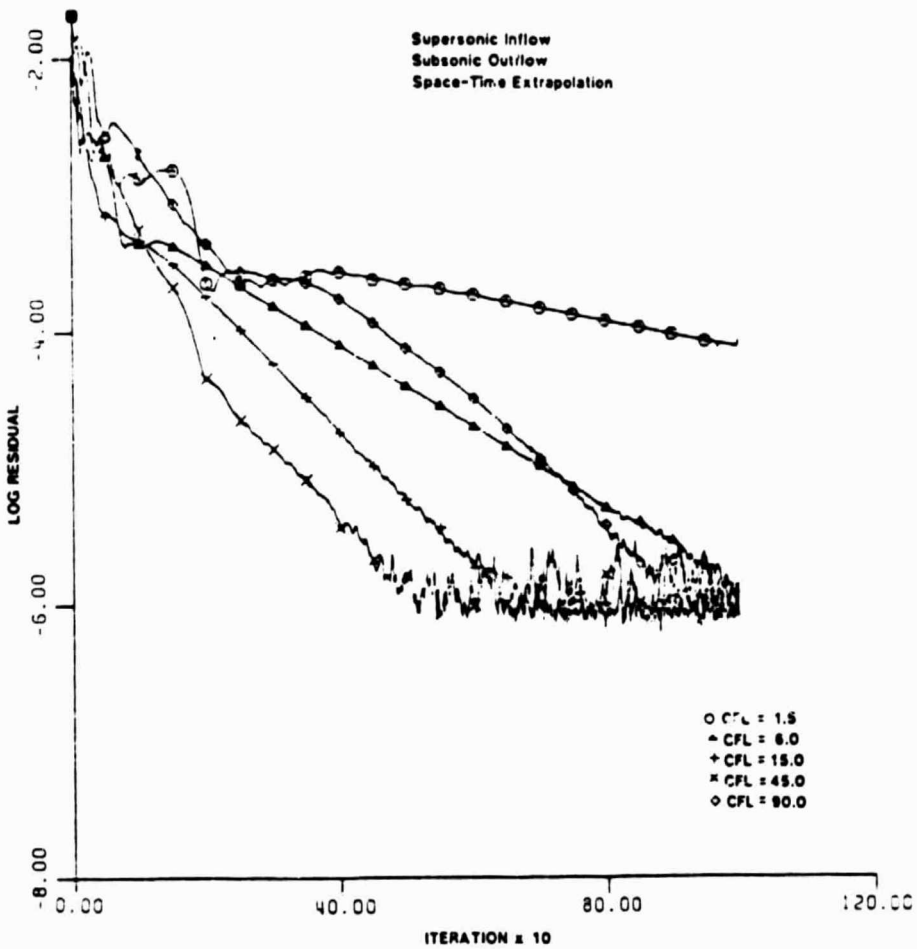

FIG. 5. Convergence history for strong shock diffuser calculation.

we found stability limits between 90 and 150. Thus the analysis in one space dimension does appear to provide a sufficient condition for stability, but it may not provide a close approximation to the stability limit. It is essential, however, to emphasize that the largest convergence rates were observed at time steps corresponding to CFL numbers of order 10 and that only a marginal computational time advantage for the implicit boundary formulations was observed.

The results for the shock-boundary layer calculation are very interesting but they demonstrate a substantial computational advantage for the implicit solid wall conditions, not for the inflow–outflow extrapolation. Here the stability boundary and the best convergence rates were observed at time step sizes corresponding to CFL_y numbers of 5 to 10. When using the implicit wall conditions, the algorithm stability appeared to be independent of grid spacing in the normal direction as might be hoped. When using the explicit wall condition, the algorithm stability was limited to a CFL_y number of about 500.

Conclusions and Discussion

While it is difficult to generalize from only a few test examples, it is apparent that a better appreciation of the role that boundary treatments play in implicit algorithms has allowed the development of far more robust Beam and Warming type solvers. For both explicit and implicit boundary treatments, we were able to compute solutions accurately with time steps 50 to 100 times larger than explicit time limits while retaining the ability to choose rather arbitrary initial conditions. In many cases, our limiting time steps for the two-dimensional test problems were in fact larger than the limit which a one-dimensional analysis would suggest.

The most important computational result we observed was that while an improved appreciation of boundary treatments did allow very large time step sizes to be used, the largest convergence rates to steady state were observed at relatively small time step sizes. For the two-dimensional test problems, the best CFL_y numbers were of order 10, not of order 100. One-dimensional test examples showed no such convergence rate behavior. Presently unpublished analysis by Abarbanel *et al.* [15] has linked this behavior to the approximate factorization form of Eqs. (2) and (3). This effect now seems to be setting the time step sizes for our viscous flow computations and new work should focus on methods for overcoming this limitation.

References

1. R. M. Beam and R. F Warming, *AIAA J.* **16** (4) (1978), 393.
2. W. R. Briley and H. McDonald, *J. Comput. Phys.* **19** (1975), 150.
3. R. W. MacCormack, "A Numerical Method for Solving the Equations of Compressible Viscous Flow," AIAA Paper 81–0110, 1980.
4. H. C. Yee, R. M. Beam, and R. M. Warming, *in* "Proc. of AIAA Computational Fluid Dynamics Conference," Paper No. 81–1009, June 1981.

5. H. O. KREISS, *Math. Comp.* **22** (1968), 703.
6. H. O. KREISS, *Proc. Roy. Soc. London Ser. A* **323** (1971), 225.
7. S. OSHER, *Trans. Amer. Math. Soc.* **137** (1969), 177.
8. S. OSHER, *Math. Comp.* **23** (1969), 335.
9. B. GUSTAFSSON, H. O. KREIS, AND A. SUNDSTRÖM, *Math. Comp.* **26** (1972), 649.
10. B. GUSTAFSSON AND J. OLIGER, "Stable Boundary Approximations for a Class of Time Discretizations of $U_t = AD_0U$." Report No. 87, Dept. of Computer Science, Upsala Univ, Sweden, September 1981.
11. H. VIVIAND, *Rech. Aerospat.* **1** (1974), 65.
12. R. M. BEAM AND R. F. WARMING, "An Implicit Factor Scheme for the Compressible Navier–Stokes Equations, II: The Numerical ODE Connection," AIAA Paper 79-1446, Williamsburg, Va., 1979.
13. S. S. ABARBANEL AND E. M. MURMAN, "Stability of Two Dimensional Hyperbolic Initial Boundary Value Problems for Explicit and Implicit Schemes," Symposium on Numerical Boundary Conditions, NASA Ames Research Center, October 1981.
14. R. C. BUGGELN, W. R. BRILEY, AND H. MCDONALD, *in* "Proceedings of AIAA Computational Fluid Dynamics Conference," Paper No. 81-1023, June 1981.
15. S. S. ABARBANEL, D. L. DWOYER, AND D. GOTTLIEB, private communication, July 1981.

RECEIVED: January 6, 1982; REVISED: June 15, 1982

W. T. THOMPKINS, JR. AND R. H. BUSH

Department of Aeronautics and Astronautics,
Massachusetts Institute of Technology,
Cambridge, Massachusetts 02139

Printed by the St. Catherine Press Ltd., Tempelhof 41, Bruges, Belgium

65M10
65N10
76A60

PROPAGATION, STABILITY AND CONVERGENCE OF WAVELIKE SOLUTIONS OF FINITE DIFFERENCE EQUATIONS WITH VARIABLE COEFFICIENTS

M. B. Giles*

W. T. Thompkins, Jr#

Massachusetts Institute of Technology

Cambridge, Massachusetts 02139

*Research Assistant, Dept. of Aeronautics and Astronautics

#Associate Professor, Dept. of Aeronautics and Astronautics

Number of pages: 18

Number of figures: 3

Running Head: Propagation of numerical waves

Send proof to:

Prof. W. T. Thompkins
Room 33-208, Dept. of Aero and Astro
Mass. Inst. of Tech.
Cambridge, MA 02139

Abstract

An asymptotic approach is used to analyze the propagation and dissipation of wavelike solutions to finite difference equations. It is shown that to first order the amplitude of a wave is convected at the local group velocity and varies in magnitude if the coefficients of the finite difference equation vary. Asymptotic boundary conditions coupling the amplitudes of different wave solutions are also derived. Equations are derived for the motion of wavepackets and their interaction at boundaries. Comparison with numerical experiments demonstrates the success and limitations of the asymptotic approach. Finally an asymptotic global stability analysis is developed.

Notation

$$\delta_x U_{j+\frac{1}{2}} = U_{j+1} - U_j \qquad \mu_x U_{j+\frac{1}{2}} = \frac{1}{2}(U_{j+1} + U_j)$$

$$\Delta_x U_j = U_{j+1} - U_j \qquad \nabla_x U_j = U_j - U_{j-1}$$

$$E_{mx} U_j = U_{j+m}$$

When there are several independent variables the subscript on the finite operator denotes the direction of the shift, differencing or averaging. For example,

if $U_j^n = u(x_j, t_n)$ then $\delta_x U_{j+\frac{1}{2}}^n = U_{j+1}^n - U_j^n$.

$\bar{A}$ = complex conjugate of A

Re(A) = Real component of A

Im(A) = Imaginary component of A

I. Introduction

Methods for analysing dispersive partial differential equations are well established. Using Fourier decomposition and asymptotic evaluation of integrals, or by direct asymptotic expansion, [5,9] it can be shown that the energy propagates at the local group velocity. Ray theory [5,9] then treats wavepackets, localized wavelike disturbances, as particles and derives simple o.d.e.'s for their motion. This paper applies the techniques to the analysis of numerical wave propagation in finite difference equations. Due to the discretization the numerical waves are always dispersive even if the analytic system being modeled is nondispersive. Until recently the importance of the group velocity in analyzing finite difference solutions does not seem to have been recognized. Kentzer [4] discusses the role of group velocity and shows that in many common schemes the numerical group velocity at high wavenumbers is in the opposite direction to the analytic group velocity. Vichnevetsky and Bowles [8] derive reflection coefficients for the interaction of waves at boundaries, and present several illustrative numerical examples. Trefethen [6] provides a group velocity interpretation of the stability theory of Gustaffson, Kreiss and Sundstrom [3],

and in a forthcoming paper [7] will derive rigorous conditions for the P-stability [10] of two-boundary problems. In the stability analysis in this paper we use P-stability, which is concerned with stability in the limit $t \to \infty$, rather than GKS-stabilty which is concerned with stability in the limit $\Delta t \to 0$. Reference [2] contains further details and numerical examples of the work in this paper. It also includes a more general global stability analysis which allows for variable coefficients in the finite difference equations, and in the case of constant coefficients reduces to the exact stability analysis of Beam, Warming and Yee [1].

The approach we use is an asymptotic one in which a wave solution is expressed as a product of a complex amplitude and an oscillatory phase function whose frequency and wavenumber may also be complex. The asymptotic assumption, or approximation, is that the length scale for variations in the amplitude and wavenumber is large relative to a mesh cell length. An asymptotic expansion leads to a local dispersion relation relating the wavenumber to the frequency. The first order terms produce an equation for the amplitude in which the local group velocity appears as the velocity of convection of the amplitude. Also there is a variation in the magnitude of the amplitude if the coefficients of the finite difference equation vary. All of the wave solutions with a given frequency and different wavenumbers are coupled at the boundaries by asymptotic boundary conditions. If there are only two waves per frequency then this reduces to the amplitude reflection coefficients computed by Vichnevetsky and Bowles [8].

The following section develops a theory for the motion of wavepackets which are wavelike disturbances of finite length and constant frequency. Using the techniques of classical ray theory [5,9], these can be treated as particles and simple o.d.e.'s can be derived to describe their motion and the change in their energy. When they reach the boundary they are reflected into wavepackets of a different wavenumber but the same frequency and the energy of the reflected wavepacket can be calculated from boundary reflection coefficients. The last section derives a global stability analysis in which the usual Fourier stability analysis is modified to calculate the effects of non-periodic boundary conditions and slowly varying coefficients. This analysis is then used to calculate the spectral radius of the backward Euler method.

II. Asymptotic Amplitude Analysis

Asymptotic Amplitude Equation

Consider a general linear homogeneous finite difference equation with variable coefficients,

$$L_j U_j^n = 0 \tag{1}$$

where

$$L_j \equiv \sum_{m,p} C_{mp}(x) E_{mx} E_{pt} \tag{2}$$

If the coefficients C_{mp} are constants then

$$U_j^n = \exp[i(j\phi - n\Omega)] \tag{3}$$

is an exact solution of (1) provided

$$\sum_{m,p} C_{mp} \exp[i(m\phi - p\Omega)] = 0 \tag{4}$$

This equation is called the dispersion relation between wavenumber ϕ and frequency Ω. If the coefficients are not constant then U can be expressed as,

$$U_j^n = A(j,n) \exp[i\Psi(j,n)] \tag{5}$$

where A(j,n) is a slowly varying amplitude and $\Psi(j,n)$ is the phase of the wave and is related to the frequency Ω and wavenumber ϕ by

$$\frac{\partial \Psi}{\partial n} = -\Omega \qquad \frac{\partial \Psi}{\partial j} = \phi \tag{6a,b}$$

The asymptotic approximation which is made is that the length scale L_A and time scale T_A for variations in A and the length scale L_ϕ for variations in ϕ are much greater than 1. Substituting (5) into (2) and expanding A and Ψ in Taylor seies about a point (j,n) yields,

$$L_j\, U_j^n = \exp[i\Psi] \sum_{m,p} C_{mp}(j) \exp[i(m\phi - p\Omega)] \left(A + m \frac{\partial A}{\partial j} + p \frac{\partial A}{\partial n} + \frac{im^2}{2} A \frac{\partial \phi}{\partial j} \right) + O(AL_A^{-2}, AT_A^{-2}, AL_\phi^{-2}) \tag{7}$$

To satisfy equation (1) the amplitude A(j,n) must satisfy ,

$$a_0(\phi,\Omega,j)\, A + a_1(\phi,\Omega,j) \frac{\partial A}{\partial n} + a_2(\phi,\Omega,j) \frac{\partial A}{\partial j} + a_3(\phi,\Omega,j)\, A \frac{\partial \phi}{\partial j} = 0 \tag{8}$$

where ,

$$a_0(\phi,\Omega,j) = \sum_{m,p} C_{mp}(j)\ \exp[i(m\phi - p\Omega)] \tag{9a}$$

$$a_1(\phi,\Omega,j) = i\left(\frac{\partial a_0}{\partial \Omega}\right)_{\phi,j\ \text{const}} \tag{9b}$$

$$a_2(\phi,\Omega,j) = -i\left(\frac{\partial a_0}{\partial \phi}\right)_{\Omega,j\ \text{const}} \tag{9c}$$

$$a_3(\phi,\Omega,j) = -\frac{i}{2}\left(\frac{\partial^2 a}{\partial \phi^2}\right)_{\Omega,j\ \text{const}} \tag{9d}$$

Because of the asymptotic assumptions (8) can only be satisfied if

$$a_0(\phi,\Omega,j) = 0 + O(\ L_0^{-1}, L_A^{-1}, T_A^{-1}\ ) \tag{10}$$

This is the asymptotic form of the dispersion relation between ϕ and Ω and will usually be satisfied by setting a_0 identically equal to zero. ϕ is now a slowly varying function of j due to the slow variation in the coefficients. Neglecting the second order terms and dividing by a_1 gives the asymptotic amplitude equation.

$$\frac{\partial A}{\partial n} + r_g \frac{\partial A}{\partial j} = \varepsilon\ A \tag{11}$$

where $r_g = a_2 / a_1$ and $\varepsilon = -(a_3 \frac{\partial \phi}{\partial j} + a_0) / a_1$ (12,13)

Differentiating Eq.(33) with j held constant gives,

$$da_0 = \left(\frac{\partial a_0}{\partial \Omega}\right)_{\phi,j\ \text{const}} d\Omega + \left(\frac{\partial a_0}{\partial \phi}\right)_{\Omega,j\ \text{const}} d\phi = 0 \tag{14}$$

Hence,

$$\left(\frac{\partial \Omega}{\partial \phi}\right)_{j\ \text{const}} = a_j / a_1 = r_g \qquad (15)$$

Thus the amplitude A of the wave is convected at the local group velocity.

Asymptotic Boundary Conditions

The general solution of Eq.(1) is a sum of waves with different constant frequencies Ω and slowly varying wavenumber ϕ and amplitude A.

$$U_j^n = \sum_{\Omega} \sum_{m=1}^{M} A_m(j,n) \exp\left[i\left(\int_0^j \phi_m(\xi)\, d\xi - n\Omega\right)\right] \qquad (16)$$

The outer summation is over different values of Ω, and the inner summation is over the M different values of ϕ which satisfy the dispersion relation for each Ω. For each Ω,m the amplitude A satisfies the asymptotic amplitude equation on the interior of the computational domain independent of all the other waves. All the waves of each frequency are however coupled by boundary conditions.

Suppose one of the finite difference boundary conditions at j=J is

$$B\, U_J^n \equiv \sum_{l,p} D_{lp}\, E_{lx}\, E_{pt}\, U_J^n = 0 \qquad (17)$$

Performing the same expansion as in the derivation of the asymptotic amplitude equation, retaining only the leading terms, and equating the coefficients of $\exp(-i\Omega)$ for each Ω, the boundary condition becomes,

$$\sum_{m=1}^{M} b(\Omega,\phi_m)\, A_m(J)\, \exp\left[i \int_0^J \phi_m \, d\xi\right] = 0 \qquad (18)$$

where,

$$b(\Omega,\phi_m) = \sum_{l,p} D_{lp} \exp(i(l\phi - p\Omega)) \qquad (19)$$

There are similar asymptotic boundary conditions at j=0.

III. Ray Theory And Wavepacket-Particles

In addition to the asymptotic approximations made earlier this section assumes that for all real wavenumbers ϕ, the frequency Ω is real for all j and so the group velocity r_g is real.

A Lagrangian-type total time derivative is defined by,

$$\frac{d}{dn} \equiv \frac{\partial}{\partial n} + r_g \frac{\partial}{\partial j} \qquad (20)$$

so $$\frac{dj}{dn} = r_g \ , \qquad (21)$$

$$\frac{dA}{dn} = \varepsilon A \ , \qquad (22)$$

and $$\frac{d\phi}{dn} = r_g \frac{\partial \phi}{\partial j} \ . \qquad (23)$$

A general initial value problem for a wave of frequency Ω and wavenumber $\phi(\Omega,j)$ can be solved by integrating these equations from given initial conditions.

A wavepacket is a wave for which the amplitude A is non-zero on only

a small part of the domain. The energy is defined to be,

$$E(n) = \int_{x_0}^{x_J} |A(x,t_n)|^2 \, dx = \int_0^J |A(j,n)|^2 \frac{dx}{dj} \, dj \tag{24}$$

Differentiating this definition, and using (22), yields,

$$\frac{dE}{dn} = \left[\epsilon + \bar{\epsilon} + \left(\frac{dx}{dj}\right)^{-1} \frac{\partial}{\partial j}\left(r_g \frac{dx}{dj}\right) \right] E \tag{25}$$

Thus equations (21) and (25) describe the motion of a wavepacket particle in the interior of the computational domain. When the wavepacket reaches a boundary it is reflected as one or more wavepackets with the same frequency but different wavenumber. For the case in which there are just two wavenumbers corresponding to the same frequency the ratio of the reflected energy E_2 to the incident energy E_1 is given by,

$$\frac{E_2}{E_1} = \left| \frac{r_g(\vartheta_2,J)}{r_g(\vartheta_1,J)} \right| \, |R_J|^2 \tag{26}$$

where the amplitude reflection coefficient R_J is defined by,

$$R_J = \frac{A_2(J,n)}{A_1(J,n)} \tag{27}$$

and is determined from the asymptotic boundary condition.

Example

The example is the solution of the model convective equation,

$$\frac{\partial u}{\partial t} + c \frac{\partial u}{\partial x} = 0 \tag{28}$$

using a trapezoidal method,

$$\left(\delta_t + \frac{1}{2} r_{j+\frac{1}{2}} \mu_t \Delta_x + \frac{1}{2} r_{j-\frac{1}{2}} \mu_t \nabla_x\right) U_j^{n+\frac{1}{2}} = 0 \tag{29}$$

$$\text{with} \quad r_{j+\frac{1}{2}} = \frac{c\Delta t}{x_{j+1} - x_j} \tag{30}$$

Figure 1 shows the solution U(x,t) corresponding to a uniform grid $0<j<200$ with r=1, and initial conditions corresponding to a wavepacket approximately 20 mesh units wide. Comparison of the heights of the wavecrests a-e at time levels 60 and 120 shows that the phase velocity, the velocity of the wavecrests, is greater than the group velocity, the velocity of the wavepacket.

Figures 2 and 3 show comparisons of the wavepacket theory with numerical experiments. In each case "experimental" values for X(n), the position of the wavepacket, and E(n), its energy, are obtained by solving the finite difference equations and "predicted" values are calculated by solving the wavepacket equations. The initial wavepacket in each case is similar to that in the previous example.

In the first case r varies exponentially from 0.05 at j=0 to 0.2 at j=200 and Ω=0.04 . Figure 2 shows X(n) and ln[E(n)] both predicted and experimental. This example shows the movement of a wavepacket and the change in its energy due to the variation in r. The agreement between the predicted and experimental values is excellent. The energy of the analytic solution is constant so the wavepacket theory has successfully predicted almost all of the change in the numerical energy due to the

nonuniform grid.

In the second case r is constant and eq[illegible] to 1.0 and η=0.3 . Figure 3 shows X(n) and ln[E(n)]. This example illustrates the effect of the downstream boundary reflecting a wavepacket with reduced energy. Because of the finite length of the wavepacket the drop in energy is smeared and X(n) does not quite reach 1.0 . Again the agreement is excellent with the wavepacket theory accurately predicting the energy of the reflected wavepacket.

IV. Asymptotic Stability and Convergence Analysis

In this section it is assumed that there are two wavenumbers corresponding to each frequency, and that if one is real then so too is the other. Examples of methods satisfying these conditions are the trapezoidal method applied to the model convective problem with variable CFL number r, and the whole class of Beam-Warming schemes applied to the model convective problem with constant CFL number.

The normal Fourier analysis assumes constant coefficients and periodic boundary conditions and derives eigenfrequencies $\Omega(\phi)$ where ϕ is a real wavenumber satisfying the periodic boundary conditions and $\Omega(\phi)$ is the corresponding frequency given by the dispersion relation. The common use of Fourier analysis to predict the stability of problems with nonperiodic boundary conditions implicitly assumes that $\Omega(\phi)$ is a close approximation to the true eigenfrequency. This section follows

that assumption, calculates a correction Ω' to the Fourier frequency $\Omega(\phi)$ due to the boundary conditions, and then determines the validity of the assumption based on the asymptotic errors.

$$U_j^n = A_1(j,n)\ \exp\left(i\int_0^j \phi_1\ d\xi - in\Omega\right) + A_2(j,n)\ \exp\left(i\int_0^j \phi_2\ d\xi - in\Omega\right) \quad (31)$$

If the true eigenfrequency is $\Omega+\Omega'$ then $A\propto\exp(-in\Omega')$ and so,

$$A_m(j,n) = \exp(-in\Omega')\ A_m(j,0) \qquad , m=1,2 \quad (32)$$

Substituting these expressions into the asymptotic amplitude equations to evaluate the time derivative and then integrating the resultant o.d.e. gives,

$$A_m(J,0) = A_m(0,0)\ \exp\int_0^J\left(\frac{\varepsilon+i\Omega'}{r_g}\right)_m dj \qquad , m=1,2 \quad (33)$$

The two asymptotic boundary conditions then become in matrix form

$$B\begin{pmatrix} A_1(0,0) \\ A_2(0,0) \end{pmatrix} = 0 \quad (34)$$

A non-trivial solution exists only if $\det(B) = 0$ and this leads to the following equation for Ω'.

$$\exp\left(i\Omega'\int_0^J [r_g(\phi_1,j)]^{-1}-[r_g(\phi_2,j)]^{-1}\ dj\right) =$$

$$\frac{b_2(\Omega,\phi_2)\ b_1(\Omega,\phi_1)}{b_2(\Omega,\phi_1)\ b_1(\Omega,\phi_2)}\ \exp\left(i\int_0^J \phi_2-\phi_1\ dj\right)\ \exp\left(\int_0^J \left(\frac{\varepsilon}{r_g}_2 - \frac{\varepsilon}{r_g}_1\right) dj\right) \quad (35)$$

If ϕ_1, ϕ_2 are chosen so that the r.h.s. is real and positive then

$$\Omega' = -\frac{i}{N}\left(\log \left| \frac{b_2(\Omega,\phi_2)\ b_1(\Omega,\phi_1)}{b_2(\Omega,\phi_1)\ b_1(\Omega,\phi_2)} \right| + \mathrm{Re} \int_0^J \left(\frac{\varepsilon}{r_{g_2}}\right) - \left(\frac{\varepsilon}{r_{g_1}}\right) dj \right) \tag{36}$$

where,

$$N = \int_0^J [r_g(\phi_1,j)]^{-1} - [r_g(\phi_2,j)]^{-1}\, dj \tag{37}$$

Thus the frequency Ω resulting from a normal Fourier analysis is corrected by an amount Ω' due to boundary conditions and variable coefficients. This approach, using Ω as an initial approximation to the actual eigenfrequency, is valid provided the asymptotic error is small. The asymptotic error is $O(L_A^{-2}, T_A^{-2}) = O(J^{-2}, \Omega'^2)$ so provided $r_g \ll J$ $N \gg 1$ and hence $\Omega' \ll 1$ except near frequencies for which

$$\left| \frac{b_2(\Omega,\phi_2)\ b_1(\Omega,\phi_1)}{b_2(\Omega,\phi_1)\ b_1(\Omega,\phi_2)} \right|$$

is zero, or infinite, which usually occurs at $\Omega=0$. However these frequencies are heavily damped by the boundary conditions and so an accurate estimate of their eigenfrequencies is not essential. This method gives accurate asymptotic values near the critical frequencies which are least damped and which therefore determine the overall spectral radius of the scheme.

Example

This example is the backward Euler method applied to the model convective problem with constant CFL number r and space extrapolation at the downstream boundary. The finite difference equation is,

$$\left(\nabla_t + r\,\mu_x\delta_x\right) U_j^{n+1} = 0 \qquad (38)$$

and the dispersion relation is,

$$a_0 = 1 - \exp(i\Omega) + ir\sin(\phi) = 0 \qquad (39)$$

After carrying out the calculations the frequency correction Ω' is found to be [2],

$$\Omega' = -\frac{ir\cos(\phi)\,(1 - ir\sin(\phi))}{2J\,(\,1 + r^2\sin^2(\phi)\,)}\,\log[\cot(\phi/2)] \qquad (40)$$

Thus the effect of the boundary conditions is to greatly accelerate convergence at low wavenumbers while having little effect on the higher wavenumbers. The spectral radius λ is

$$\lambda = \max_{\phi} |\exp(-i(\Omega+\Omega'))|$$
$$\approx 1 - \frac{r\log(J)}{4J} \qquad \text{for } J>>r \qquad (41)$$

V. Conclusions

The validity of the asymptotic approach developed in this paper is demonstrated by the numerical results in sectic III. The limitations of the wavepacket theory are due to the asymptotic approximations

involved in treating the wavepacket as a particle. The stability analysis in section IV uses fewer approximations and so the asymptotic errors will be substantially smaller.

The calculation of the asymptotic amplitude equation and asymptotic boundary conditions for a particular case is no more difficult than a normal Fourier analysis. For applicable cases the wavepacket theory and the stability analysis are straightforward. In more complex cases the main benefit from the theory is the insight given by the asymptotic amplitude equation and boundary conditions. The amplitude equation gives the group velocity and the effect of varying coefficients which is of great interest since in 2-D cascade geometries cell lengths can vary by factors of up to 100 in inviscid calculations and 1000 in viscous calculations. The asymptotic boundary conditions give the amplitude reflection coefficients which provide a practical criterion for choosing the best numerical boundary conditions.

Acknowledgments

This research was supported by NASA Lewis Research Center under grant No. NAG3-9 with Technical Monitor Dr. R. V. Chima, and by a Scholarship for M. Giles from the Kennedy Memorial Trust.

References

1 R. Beam, R. Warming, H. Yee, "Stability Analysis for Numerical Boundary Conditions and Implicit Difference Approximations of Hyperbolic Equations", Proc. NASA Symp. on Numerical Boundary Procedures, 1981, pp.99-207.

2 M. Giles and W.T. Thompkins Jr. , "Asymptotic Analysis of Numerical Wave Propagation In Finite Difference Equations" , MIT Gas Turbine and Plasma Dynamics Laboratory Report No. 171 , February 1983

3 B. Gustafsson, H-O. Kriess, A. Sundstrom, "Stability Theory of Difference Approximations for Initial Boundary Value Problems II", Math. Comp. 26 (1972), pp. 649-686.

4 C.P. Kentzer , "Group Velocity And Propagation Of Numerical Errors" , AIAA Paper No. 72-153

5 J. Lighthill , Waves In Fluids , pp 237-260 , Cambridge Univerity Press 1978.

6 L.N. Trefethen, "Group Velocity Interpretation of the Stability Theory of Gustafsson, Kreiss and Sundstrom", Jour. Comp. Phys. 49 (1983), pp. 199-217

7 L.N. Trefethen, "Stability of Finite Difference Models Containing Two or More Boundaries", to appear

8 R. Vichnevetsky and J. Bowles , Fourier Analysis of Numerical Approximations of Hyperbolic Equations , SIAM Studies In Applied Mathematics 1982.

9 G.B. Whitham , Linear And Nonlinear Waves , chapter 11 , John Wiley & Sons 1974.

10 H. Yee, R. Beam, R. Warming, "Stable Boundary Approximations for a Class of Implicit Schemes for the One-dimensional Inviscid Equations of Gas Dynamics", AIAA-81-1009-CF , AIAA Computational Fluid Dynamics Conference, Palo Alto, June 22-23, 1981

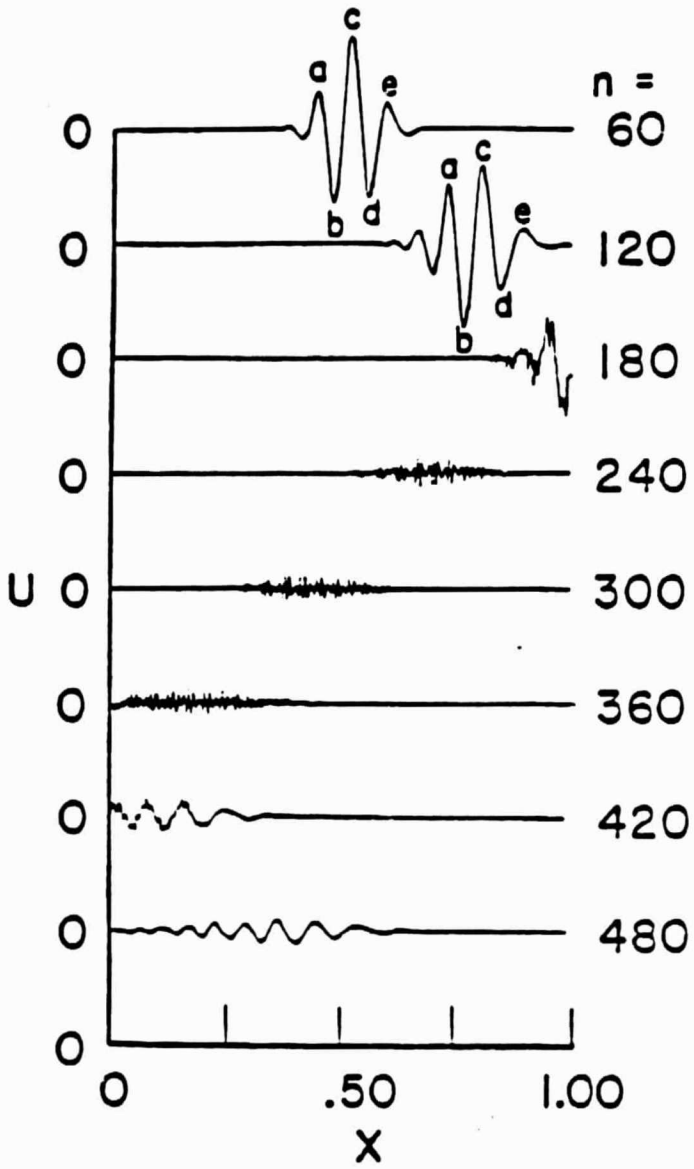

Figure 1. Numerical Solution of Convection Equation

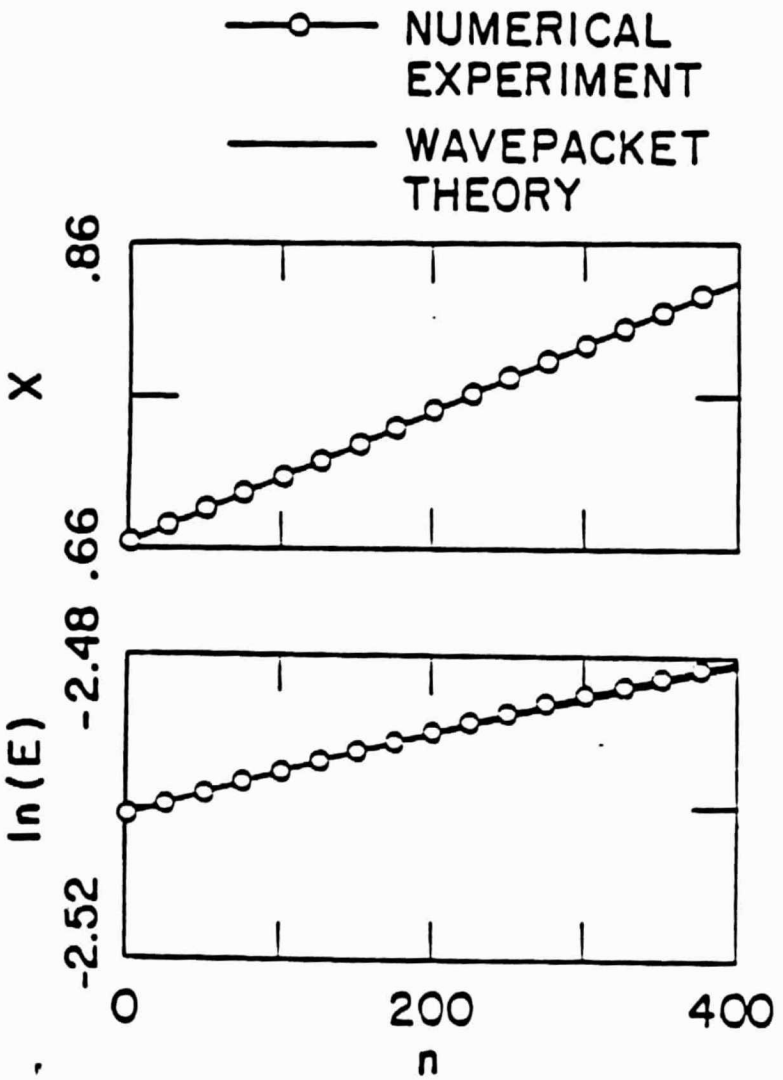

Figure 2. Position and Energy of Wavepacket: Effect of Non-Constant CFL Number

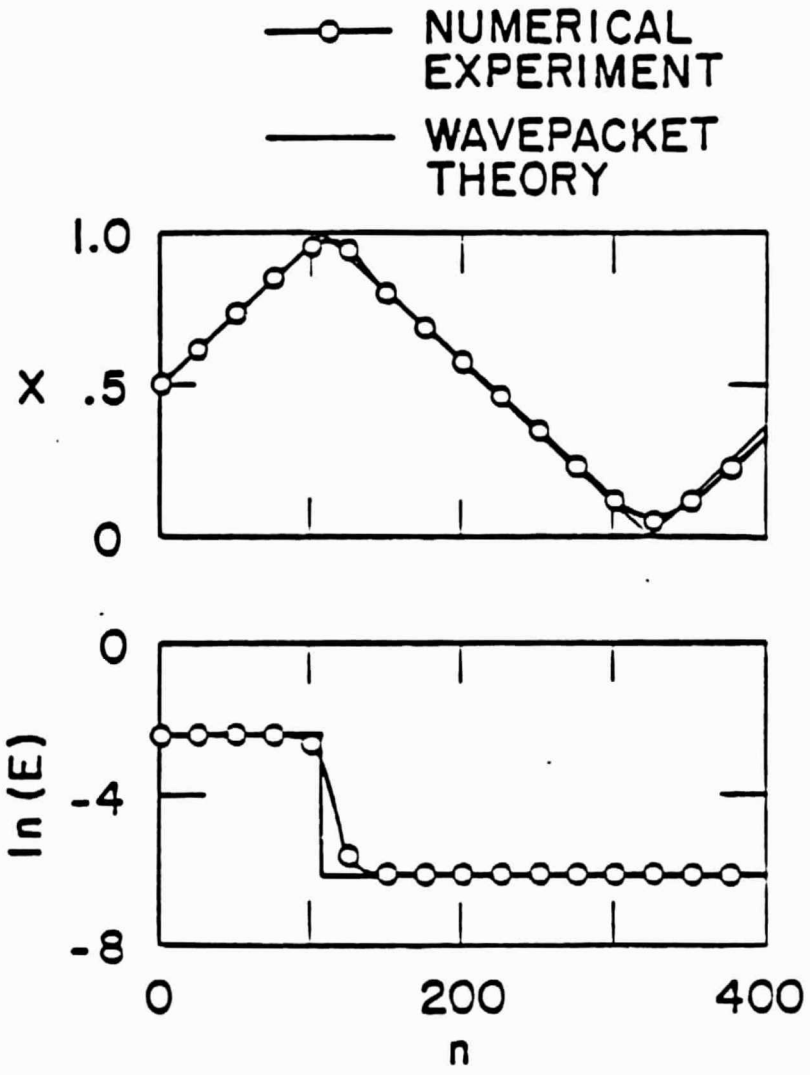

Figure 3. Position and Energy of Wavepacket: Reflections at Boundaries

14

INTERNAL REFLECTION DUE TO A NONUNIFORM GRID

Michael Giles
W. T. Thompkins, Jr.

Massachusetts Institute of Technology
Cambridge, MA 02139
Tel: 617-253-2276

Abstract

This paper presents and analyzes two examples of wave-trapping, the internal reflection of numerical waves due solely to variations in grid stretching. In both examples the analytic equation is the scalar convection equation which is non-dispersive and for which each Fourier component of a general disturbance propagates at the same velocity $c>0$. However, numerical approximations of this equation using 3-point spatial differencing and trapezoidal (or Crank-Nicholson) time integration have the property that for a given frequency there is a minimum required spatial resolution Δx for traveling wave solutions. In both the examples presented, an initially well resolved wavepacket propagates towards a region of the grid in which the spacing Δx is increasing, until it reaches the point at which the spatial resolution reaches the critical value and its group velocity is zero. It is then reflected and becomes a wavepacket with wavelength less than 4 node points traveling with negative group velocity. It travels through the well-resolved region until once again it reaches a region of inadequate grid resolution, and is then reflected back into a wavepacket with wavelength greater then 4 node points and a positive group velocity. The difference between the two examples lies in the details of the spatial differencing, which causes no qualitative change but greatly affects the "energy" of the wavepacket during the oscillation.

These two cases are analyzed using a previously derived asymptotic analysis which calculates simple o.d.e.'s for the motion and the energy change of wavepackets traveling through nonuniform domains. Despite the presence of the turning points at which the simple asymptotic analysis is not strictly valid, the agreement between the numerical experiments and the theoretical analysis is excellent.

Notation

u	variable	analytic
x,t	coordinates	analytic
c	velocity	analytic
U	variable	computational
j,n	coordinates	computational
r	velocity	computational
r_g	group velocity	computational
A	amplitude	computational
γ	phase	computational
Ω	frequency	computational
ϕ	wavenumber	computational

$$U_j^n = u(x_j, t_n)$$

$$E_{mx} U_j^n = U_{j+m}^n \quad , \quad E_{pt} U_j^n = U_j^{n+p}$$

$$\Delta_x U_j^n = U_{j+1}^n - U_j^n \quad , \quad \nabla_x U_j^n = U_j^n - U_{j-1}^n$$

$$\delta_t U_j^{n+\frac{1}{2}} = U_j^{n+1} - U_j^n \quad , \quad \mu_t U_j^{n+\frac{1}{2}} = \tfrac{1}{2}\left(U_j^{n+1} + U_j^n\right)$$

I. Introduction

Nonuniform grids are a common feature of many numerical calculations. For example, in calculating two-dimensional transonic flow over an airfoil, the grid spacing Δx will usually be very small near the leading edge of the airfoil to resolve large gradients, and around the shock to limit the errors due to numerical dissipation, while in the far field Δx often becomes very large. There is numerical evidence that these nonuniform grids can cause some problems. Grosch and Orszag [2] found spurious non-physical internal reflections due to grid stretching. Hence there is interest in analyzing simple model problems to gain insight into the difficulties.

There are two limiting cases of non-uniform grids. In the first there are two uniform grids with different spatial resolution Δx joined by an interface. This case has been analyzed by Vichnevetsky [6] and Trefethen [5]. To summarize their findings, in general a wave incident on the interface produces a reflected wave in addition to a transmitted wave. If the wavelength of the wave is much larger than Δx on both sides, then the reflected wave has a very small amplitude. If the wavelength is of the same order as Δx then up to 100% of the numerical energy is reflected from the interface.

In the second case Δx varies slowly over a length scale much larger than Δx. It is this case which is considered here using a previously derived asymptotic analysis [1]. This analysis is also applicable to finite difference equations in which the non-uniform coefficients are due not to non-uniform grids but to slowly varying analytic equations. First we review the theory for the asymptotic analysis and then we present two numerical solutions of the model convection equation using 3-point spatial differencing and trapezoidal (or Crank-Nicholson) time integration. Because of the particular choice of variable grid spacing Δx and the frequency of the wavepacket chosen for initial conditions, the examples both exhibit wave-trapping in which the wavepacket's motion is confined to a central portion of the domain and its position, wavenumber and energy go through a periodic oscillation. It is shown that the

asymptotic theory accurately predicts this behavior.

II. Review of Asymptotic Analysis

Consider a general linear, homogeneous, finite difference equation with variable coefficients,

$$L_j U_j^n = 0 \tag{1}$$

where

$$L_j = \sum_{m,p} C_{mp}(j)\, E_{mx}\, E_{pt} \tag{2}$$

Following the asymptotic approach of classical analysis of wave propagation in nonuniform dispersive mediums, we consider the trial solution,

$$U_j^n = A(j,n)\exp[i\gamma(j,n)] \tag{3}$$

where $A(j,n)$ is a slowly varying amplitude and $\gamma(j,n)$ is the phase of the wave and is related to the frequency Ω and wavenumber ϕ by

$$\frac{\partial\gamma}{\partial n} = -\Omega \quad , \qquad \frac{\partial\gamma}{\partial j} = \phi \tag{4,5}$$

The asymptotic approximation which is made is that the length scale L for variations in A and ϕ is much greater than 1. Substituting (3) into (1), expanding A and γ in a Taylor series about a point (j,n), and neglecting terms of order L^{-1}, produces,

$$a_0 A + a_1\frac{\partial A}{\partial n} + a_2\frac{\partial A}{\partial j} + a_3 A\frac{\partial\phi}{\partial j} = 0 \tag{6}$$

where,

$$a_0 = \sum_{m,p} C_{mp}(j)\exp[i(m\phi - p\Omega)] \tag{7}$$

$$a_1 = i\frac{\partial a_0}{\partial\Omega} \quad , \quad a_2 = -i\frac{\partial a_0}{\partial\phi} \quad , a_3 = -\frac{1}{2}\frac{\partial^2 a_0}{\partial\phi^2} \quad . \tag{8-10}$$

All of the terms in (6) except for the first are of order L^{-1}, and so we require that the O(1) term in a_0 is identically equal to zero. Since Ω is assumed to be constant, because the coefficients in (2) are not time-varying, this condition defines the dispersion equation $\phi=\phi(\Omega,j)$. Equation (6) can then be rearranged to form the asymptotic amplitude equation.

$$\frac{\partial A}{\partial n} + r_g\frac{\partial A}{\partial j} = \epsilon A \tag{11}$$

where,

$$r_g = a_2/a_1 = \left(\frac{\partial\Omega}{\partial\phi}\right)_{j\ \mathrm{const}} \tag{12}$$

$$\epsilon = -(a_3\frac{\partial\phi}{\partial j}+a_0)/a_1 = -ia_3\frac{\partial a_0}{\partial j}/a_1 a_2 - a_0/a_1 \tag{13}$$

Thus the amplitude A of the wave is convected at the local group velocity and grows or decays in nonuniform cases in which the wavenumber ϕ is a function of j.

We now restrict our attention to non-dissipative numerical schemes for modeling hyperbolic systems. In these cases the group velocity for the numerical scheme is real, and it is convenient to define a Lagrangian-type total time derivative,

$$\frac{d}{dn} = \frac{\partial}{\partial n} + r_g\frac{\partial}{\partial j} \tag{14}$$

so that, as in classical ray theory [8], a set of equations may be written for the wave propagation along rays.

$$\frac{dj}{dn} = r_g \quad , \tag{15}$$

$$\frac{dA}{dn} = \epsilon A \quad , \tag{16}$$

$$\frac{d\phi}{dn} = r_g\frac{\partial\phi}{\partial j} \quad . \tag{17}$$

A general initial value problem for a wave of frequency Ω and wavenumber $\phi(\Omega,j)$ can be solved by integrating these equations from given initial conditions. In [4] Trefethen derived the kinematic ray equations (15),(17) from the dispersion relation for an anisotropic 2-D case in which the grid was uniform but the analytic coefficients were not. Computational experiments confirmed the predictions of the ray theory. In this paper we are interested in the motion of wavepackets, which are waves for which A is zero on all but a small part of the domain. The energy is defined to be,

$$E(n) = \int_{x_0}^{x_J} |A(x,t_n)|^2\, dx$$

$$= \int_0^J |A(j,n)|^2\frac{dx}{dj}\, dj \tag{18}$$

Differentiating this definition, and using (16), yields,

$$\frac{dE}{dn} = \left[2\mathrm{Re}(\epsilon)+\left(\frac{dx}{dj}\right)^{-1}\frac{\partial}{\partial j}\left(r_g\frac{dx}{dj}\right)\right]E \tag{19}$$

Thus equations (15), (17) and (19) describe the motion of a wavepacket in the interior of the computational domain.

III. Examples and Analysis

Both of the numerical examples are solutions to the model convective equation with constant positive velocity c.

$$\frac{\partial u}{\partial t} + c\frac{\partial u}{\partial x} = 0 \tag{20}$$

Both schemes use trapezoidal time integration and 3-point spatial differencing on a nonuniform grid. The difference between the schemes lies in the exact details of the spatial differencing. The first scheme is,

$$\left(\delta_t + \frac{1}{2}(r_{j+\frac{1}{2}}+r_{j-\frac{1}{2}})u_t(\gamma_x+\delta_x)\right)U_j^{n+\frac{1}{2}} = 0 \tag{21}$$

$$\text{with} \quad r_{j+\frac{1}{2}} = \frac{c\Delta t}{x_{j+1}-x_j} \tag{22}$$

This is only first order accurate on non-uniform grids. The second scheme is second order accurate.

$$\left(\delta_t + \frac{(r_{j+\frac{1}{2}})^2}{r_{j+\frac{1}{2}}+r_{j-\frac{1}{2}}}u_t\delta_x + \frac{(r_{j-\frac{1}{2}})^2}{r_{j+\frac{1}{2}}+r_{j-\frac{1}{2}}}u_t\gamma_x\right)U_j^{n+\frac{1}{2}} = 0 \tag{23}$$

Both examples use a computational domain with 200 nodes, and non-uniform stretching such that r varies as shown in figure 1. The initial condition is a wavepacket located at

the center of the domain, with a wavelength of approximately 12 node points.

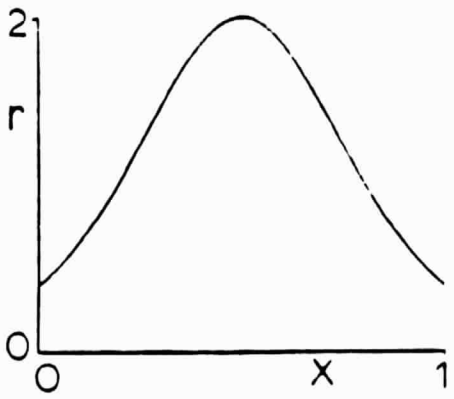

Figure 1. Plot of r(x) for both examples.

Figures 2 and 3 show the development of the solution for the two examples. Qualitatively the behavior in both cases is the same. For the first 100 iterations the wavepacket travels right, with increasing computational wavenumber as the local mesh spacing Δx increases. As the wavenumber increases past $\pi/2$, the wavepacket reverses direction, and in the next 100 iterations travels back to the center of the domain and the wavenumber reaches a peak of nearly π. The wavenumber then begins to decrease while the wavepacket continues moving left. After about 300 iterations the wavenumber is back to $\pi/2$, and the wavepacket reverses direction again and travels right back to the center of the domain, at which time it has the same wavenumber it had originally.

The analysis of the first example begins by calculating the dispersion relation.

$$a_0 = -2i \sin(\Omega/2) + ir \cos(\Omega/2)\sin(\phi) \qquad (24)$$

so the dispersion relation is,

$$2 \tan(\Omega/2) = r \sin(\phi) \qquad (25)$$

For a particular value of Ω the dispersion relation shows that there are two values of ϕ for each value of r. If r is less than a critical value $r_{crit}=2\tan(\Omega/2)$, both roots are real with one in the interval $[0,\pi/2]$ and the other in the interval $[\pi/2,\pi]$. If r is greater than r_{crit}, both roots are complex. A full discussion of these features is given in [1]. For the example presented here $r<r_{crit}$ in the middle 80% of the domain. Figure 4 shows the real roots ϕ in this part of the domain.

The wavepacket equations for the first example are,

$$\frac{dj}{dn} = r_g = r \cos(\phi)\cos^2(\Omega/2) \qquad (26)$$

$$\frac{d\phi}{dn} = -\frac{dr}{dj} \sin(\phi)\cos^2(\Omega/2) \qquad (27)$$

$$\frac{dE}{dn} = 0. \qquad (28)$$

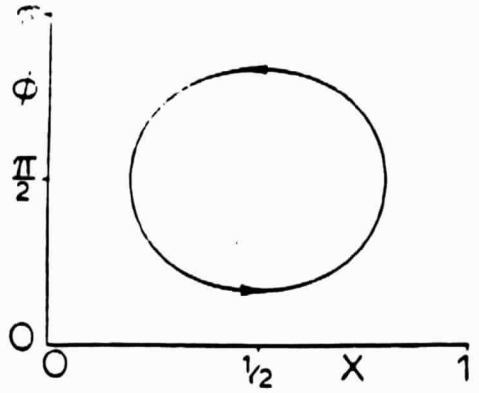

Figure 4. Wavepacket path in x-ϕ phase plane

Equations (26) and (27) describe an anticlockwise motion around the x-ϕ curve in figure 4. At the turning points $r=r_{crit}$, $\phi=\pi/2$ and the group velocity r_g is zero. $\frac{d\phi}{dn}$ however is non-zero so the wavepacket continues moving round the curve.

Figure 5 shows a comparison of the position and energy of the wavepacket obtained from the numerical experiment and from integrating the wavepacket equations. The agreement is surprisingly good considering that the theory is asymptotic, not exact. In fact the asymptotic theory is not strictly valid at the turning points, but following the procedure used by Lighthill [3] to analyze caustics (turning points in analytic equations) it is possible to construct a local analysis in the neighborhood of the turning point, which resolves this difficulty.

In the second example,

$$a_0 = -2i \sin(\Omega/2) + ir \cos(\Omega/2)\sin(\phi) + \frac{dr}{dj} \cos(\Omega/2)[\cos(\phi)-1] + O(L^{-2}) \qquad (29)$$

To first order in L this is the same as in the first example, so the dispersion equation and the equations for changes in x and ϕ are all the same. The energy equation however is different.

$$\frac{dE}{dn} = 2\frac{dr}{dj}[1-\cos(\phi)]\cos^2(\Omega/2)\,E \qquad (30)$$

Figure 6 shows the comparison between the numerical experiment and the wavepacket theory. The theory accurately predicts the large change in the energy of the wavepacket during the oscillation.

It might be argued that to calculate the stability of the finite difference scheme one should really analyze the eigenmodes of the finite difference equations. In [1] it was shown that for a particular class of problems the average decay rate calculated using the wavepacket analysis is asymptotically equal to the decay rate of the eigenmodes. Using a similar analysis it can be proved that the same is true for this problem, and so since the wavepackets have zero average decay rate, the eigenmodes also have zero decay rate. To demonstrate this this numerically, and examine the transition from a wavepacket form into an eigenmode representation example 1

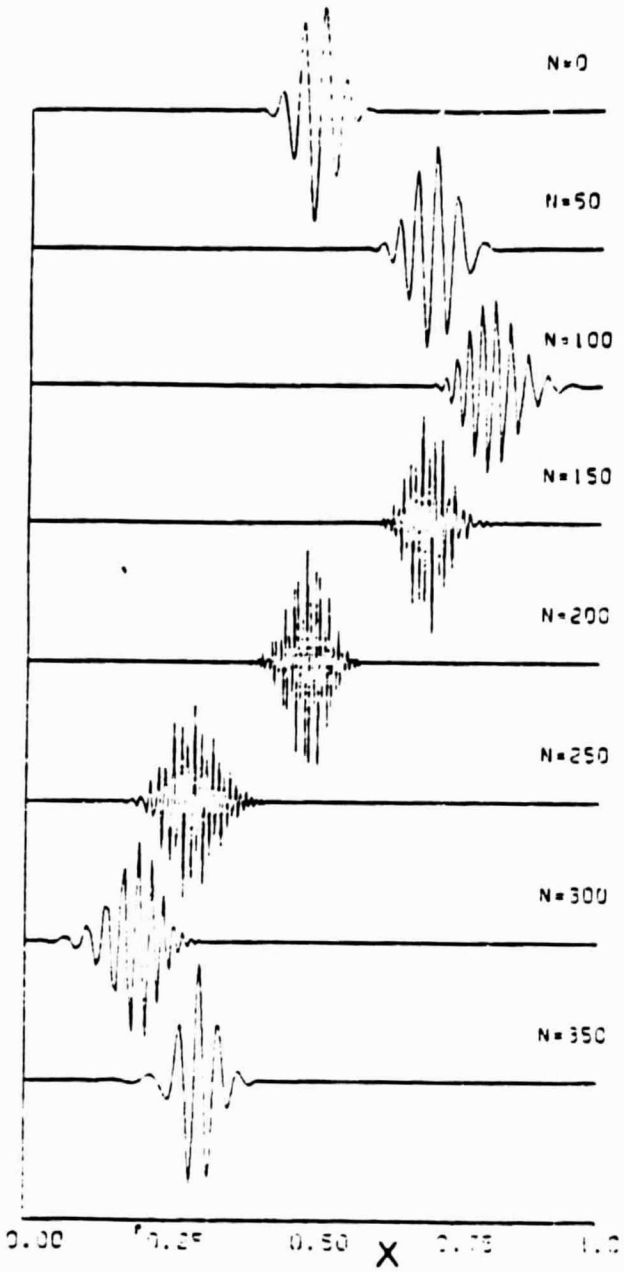

Figure 2. Plots of U^n for example 1.

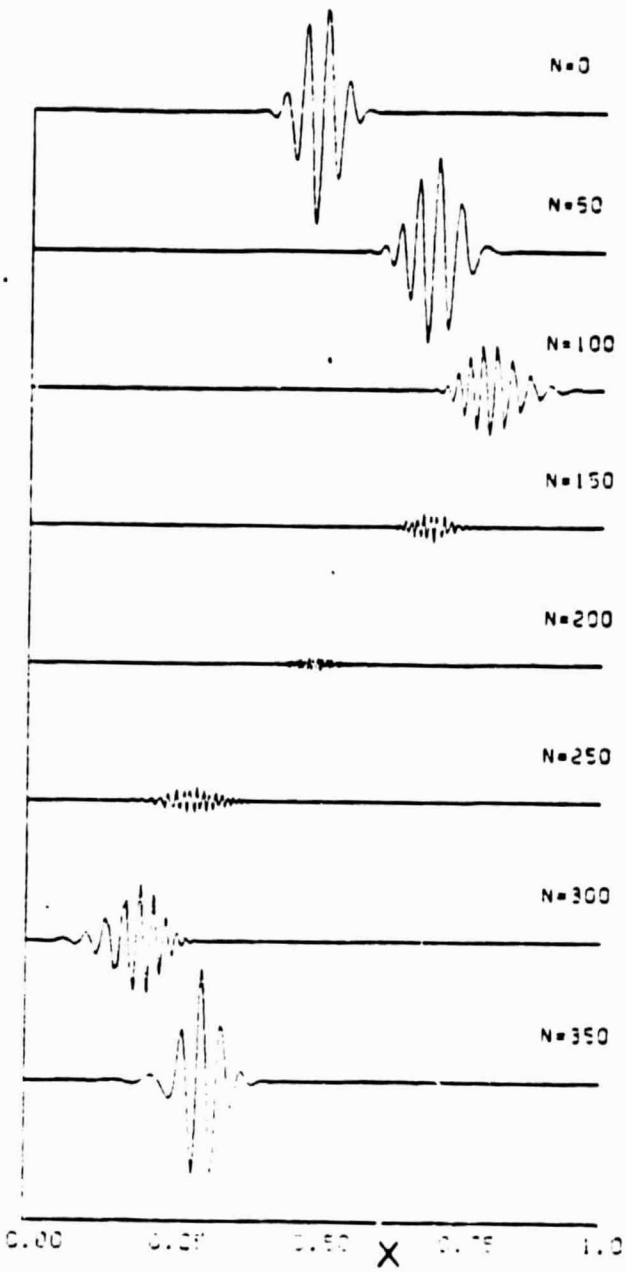

Figure 3. Plots of U^n for example 2.

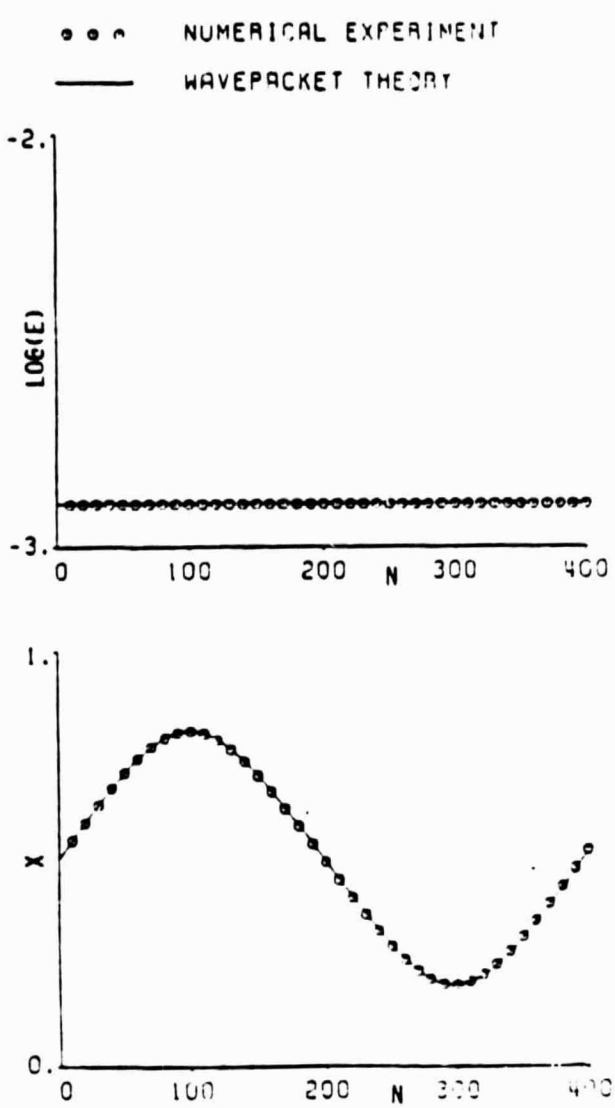

Figure 5. Comparison between theory and experiment for example 1.

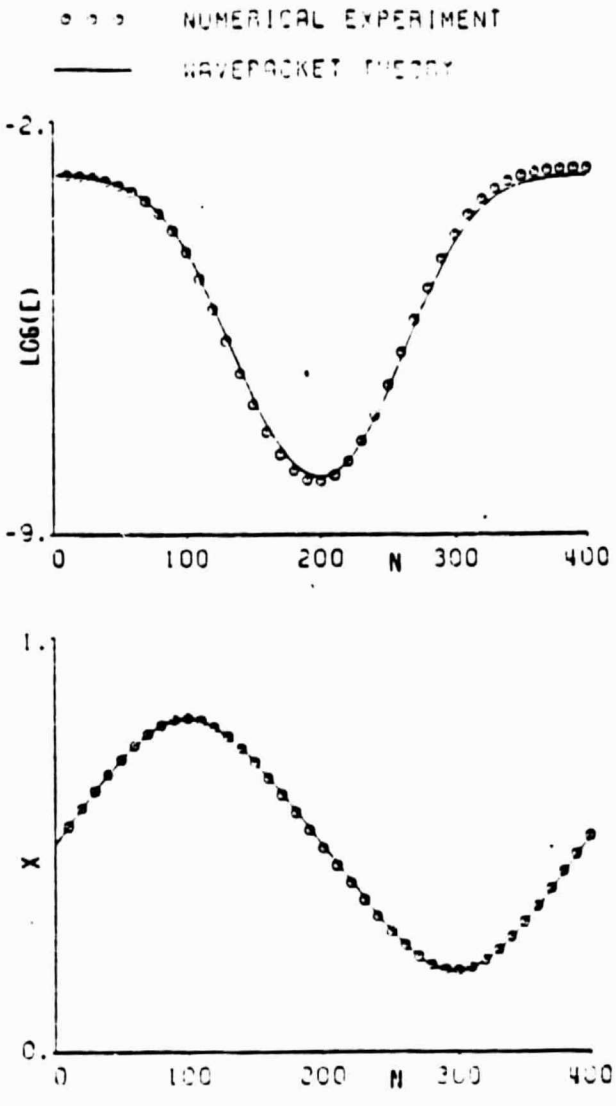

Figure 6. Comparison between theory and experiment for example 2.

was continued for 80,000 iterations. Figure 7 shows the solution at various stages in its development. 1000 iterations represent 2.5 periods of the oscillation, so in figure 7(a) the wavepacket is alternately traveling left then right. Gradually the wavepacket becomes stretched with the largest amplitude at the front of the wavepacket and a steadily growing "tail" behind. This is a more extreme example of a phenomenon noted and discussed by Vichnevetsky [7]. In the original wavepacket the amplitude modulation corresponds to a small perturbation in the frequency, and consequently there is energy associated with slightly higher frequencies which travels at a smaller group velocity than the majority of the energy. After about 50,000 iterations the energy is spread throughout the region in which $r > r_{crit}$. At this stage in the development the solution is best considered to be a sum of eigenmodes of the system. Since there are probably several eigenmodes with frequencies close to the frequency of the original wavepacket, there is considerable "beating" or interference between the eigenmodes.

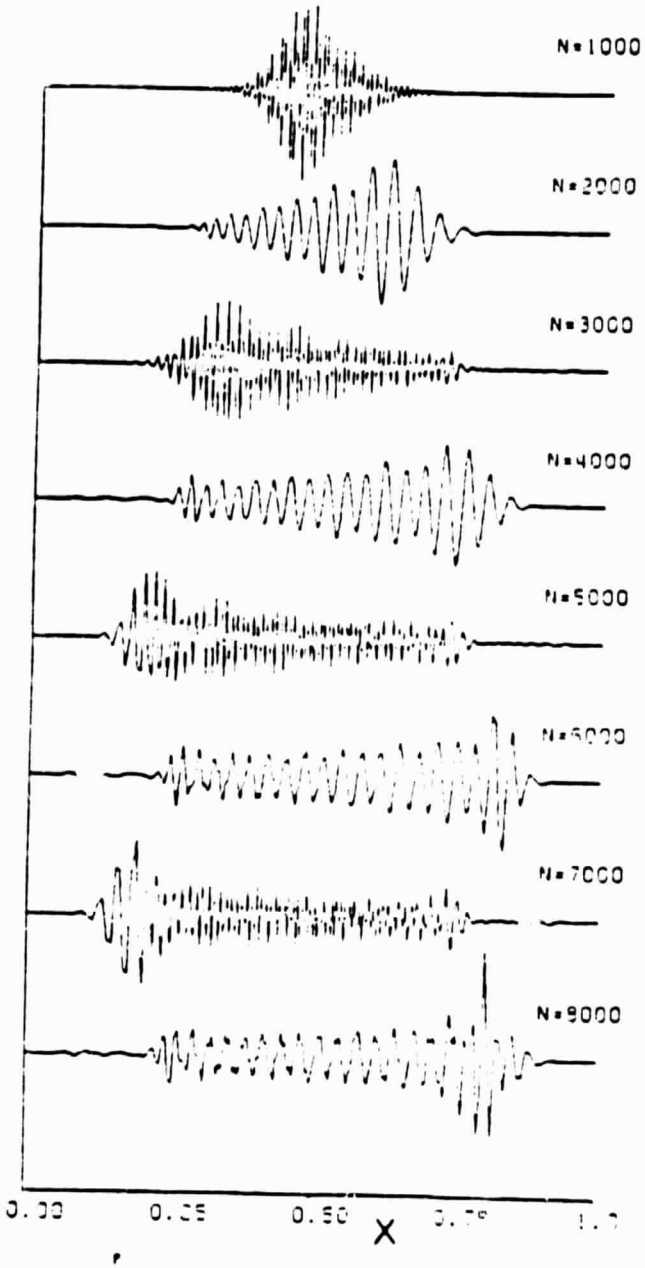

Figure 7a. Continuation of example 1.

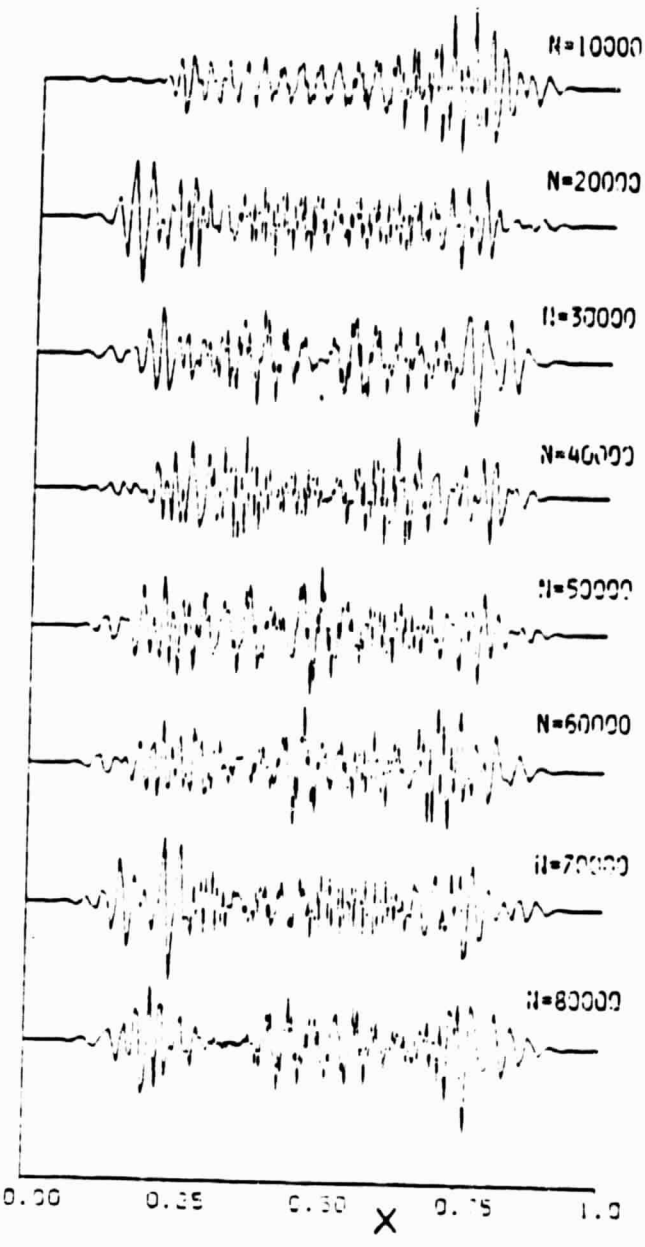

Figure 7b. Continuation of example 1.

Acknowledgments

This research was supported by NASA Lewis Research Center under grant No. NAG3-9, with Technical Monitor Dr. R. V. Chima.

References

1 M. Giles and W.T. Thompkins Jr., "Asymptotic Analysis of Numerical Wave Propagation In Finite Difference Equations," MIT Gas Turbine and Plasma Dynamics Laboratory Report No. 171 , February 1983.

2 C. Grosch and S. Orszag, "Problems in Unbounded Domains," Jour. Comp. Phys. 25 (1977), pp. 273-296.

3 J. Lighthill, Waves In Fluids, Cambridge Univerity Press, 1978.

4 L.N. Trefethen, "Group Velocity in Finte Difference Schemes," SIAM Review, Vol. 24, No. 2, April 1982.

5 L.N. Trefethen, "Wave Propagation and Stability for Finite Difference Schemes," Ph.D. Dissertation, Dept. of Comp. Sci., Stanford University, 1982.

6 R. Vichnevetsky, "Propagation Through Numerical Mesh Refinement For Hyperbolic Equations," Mathematics and Computers in Simulation XXIII (1981) pp. 344-353.

7 R. Vichnevetsky and B. Peiffer, "Error Waves in Finite Element and Finite Difference Methods for Hyperbolic Equations," Advances in Computer Methods for Partial Differential Equations, R. Vichnevetsky (Editor), 1975.

8 G.B. Whitham , Linear And Nonlinear Waves, chapter 11 , John Wiley & Sons, 1974.

NASA Contractor Report

ICASE

EIGENMODE ANALYSIS OF UNSTEADY
ONE-DIMENSIONAL EULER EQUATIONS

Michael Giles

NASA Contract No. NAS1-17130
August 1983

INSTITUTE FOR COMPUTER APPLICATIONS IN SCIENCE AND ENGINEERING
NASA Langley Research Center, Hampton, Virginia 23665

Operated by the Universities Space Research Association

National Aeronautics and
Space Administration

Langley Research Center
Hampton, Virginia 23665

EIGENMODE ANALYSIS OF UNSTEADY ONE-DIMENSIONAL EULER EQUATIONS

Michael Giles
Massachusetts Institute of Technology

Abstract

The initial boundary value problem describing the evolution of unsteady linearized perturbations of a steady, uniform subsonic flow is analyzed. The eigenmodes and eigenfrequencies of the system are derived and several examples are presented to illustrate the effect of different boundary conditions on the exponential decay rate of the eigenmodes. The resultant implications for the stability and convergence rates of finite difference computations are discussed.

Research was supported in part by the National Aeronautics and Space Administration under NASA Contract No. NAS1-17130 and NASA Grant No. NAG3-9 while the author was in residence at the Institute for Computer Applications in Science and Engineering, NASA Langley Research Center, Hampton, VA 23665.

INTRODUCTION

In finite difference calculations of steady-state subsonic solutions of quasi-one-dimensional and two-dimensional Euler equations using time marching methods, it is often observed that when the solution has almost converged to steady-state the remaining residual is due to the propagation of low frequency waves up and down the domain. These waves are largely unaffected by numerical viscosity and are dissipated through the interaction with the inflow and outflow boundary conditions. The purpose of this paper is to examine this process by analyzing the unsteady linearized perturbations of a one-dimensional, steady, uniform, subsonic flow. For this linear problem with constant coefficients it is possible to derive the exact eigenmodes and eigenfrequencies of the initial boundary value problem. This is the classical technique used to analyze physical and acoustical vibrations in a finite domain [5] and more recently used in numerical analysis to examine the P-stability of finite difference approximations to scalar equations [2,3]. The exponential decay rate of the physical eigenmodes is computed for several different sets of boundary conditions commonly used in finite difference calculations and the implications for the stability and convergence rates of these calculations are discussed.

The wellposedness of both the initial boundary value problem (i.b.v.p.) and the steady-state boundary value problem (b.v.p.) is discussed briefly. The definitive analysis of the i.b.v.p. for multi-dimensional hyperbolic systems is given by Kreiss in [4]. Oliger and Sundström [7], use an energy method to establish sufficient conditions for the wellposedness of the Euler i.b.v.p. Finally, the wellposedness of the steady-state solution to the nonlinear quasi-one-dimensional and two-dimensional Euler equations will be discussed in a forthcoming paper by Wornom and Hafez [9].

2. ANALYSIS

The equation for the unsteady linearized perturbation of a steady, uniform one-dimensional flow is,

$$\begin{pmatrix} \tilde{\rho} \\ \tilde{u} \\ \tilde{p} \end{pmatrix}_T + \begin{pmatrix} \bar{u} & \bar{\rho} & 0 \\ 0 & \bar{u} & \bar{\rho}^{-1} \\ 0 & \gamma\bar{p} & \bar{u} \end{pmatrix} \begin{pmatrix} \tilde{\rho} \\ \tilde{u} \\ \tilde{p} \end{pmatrix}_X = 0 , \qquad (1)$$

where $\tilde{\rho}$, $\tilde{u}$, $\tilde{p}$ are the perturbation density, velocity and pressure and $\bar{\rho}$, $\bar{u}$, $\bar{p}$ are the steady, uniform values.

The analysis is greatly simplified by defining the following non-dimensional variables

$$\rho = \tilde{\rho}/\bar{\rho} \qquad (2)$$

$$u = \tilde{u}/\bar{c} \qquad (3)$$

$$p = \tilde{p}/\bar{\rho}\,\bar{c}^2 \qquad (4)$$

$$x = X/L \qquad (5)$$

$$t = T\bar{c}/L, \qquad (6)$$

where $\bar{c} = [\gamma\bar{p}/\bar{\rho}]^{1/2}$ is the speed of sound. L is the physical length of the domain considered, so in the non-dimensional domain the subsonic inflow is at $x = 0$ and the outflow is at $x = 1$.

The resultant non-dimensional equation is

$$\begin{pmatrix} \rho \\ u \\ p \end{pmatrix}_t + A \begin{pmatrix} \rho \\ u \\ p \end{pmatrix}_x = 0, \qquad (7)$$

where

$$A = \begin{pmatrix} M & 1 & 0 \\ 0 & M & 1 \\ 0 & 1 & M \end{pmatrix}, \tag{8}$$

and M is the Mach number of the unperturbed flow.

Equation (7) has wave-like solutions

$$\begin{pmatrix} \rho \\ u \\ p \end{pmatrix} = \exp[i(kx - \omega t)]U \tag{9}$$

provided

$$(kA - \omega I)U = 0, \tag{10}$$

so ω/k is an eigenvalue of A and U is the corresponding eigenvector. The three eigenvalues of A and their corresponding eigenvectors are

$$\lambda_1 = M \qquad U_1 = \begin{pmatrix} 1 \\ 0 \\ 0 \end{pmatrix}, \tag{11a,b}$$

$$\lambda_2 = M + 1 \qquad U_2 = \begin{pmatrix} 1 \\ 1 \\ 1 \end{pmatrix}, \tag{12a,b}$$

$$\lambda_3 = M - 1 \qquad U_3 = \begin{pmatrix} 1 \\ -1 \\ 1 \end{pmatrix}. \tag{13a,b}$$

A general eigenmode of the initial boundary value problem can be written as a sum of the three eigenwaves,

$$U = e^{-i\omega t}[\alpha_1 e^{i(\omega/\lambda_1)x} U_1 + \alpha_2 e^{i(\omega/\lambda_2)x} U_2 + \alpha_3 e^{i(\omega/\lambda_3)x} U_3]. \tag{14}$$

The eigenfrequency ω and the values of the constants α_1, α_2, α_3 are determined by the three boundary conditions.

At the inflow boundary at $x = 0$ there are two boundary conditions which when linearized and non-dimensionalized have the form,

$$C_{in}\, U = 0, \tag{15}$$

where C_{in} is a 2×3 matrix. Substitution of (14) into (15) yields the equation,

$$\begin{pmatrix} b_{11} & b_{12} & b_{13} \\ b_{21} & b_{22} & b_{23} \end{pmatrix} \begin{pmatrix} \alpha_1 \\ \alpha_2 \\ \alpha_3 \end{pmatrix} = 0 \tag{16}$$

where

$$\begin{pmatrix} b_{11} & b_{12} & b_{13} \\ b_{21} & b_{22} & b_{23} \end{pmatrix} = C_{in} \begin{pmatrix} U_1 & U_2 & U_3 \end{pmatrix}. \tag{17}$$

A necessary condition for the initial boundary value problem to be wellposed is that the 2×2 matrix

$$\begin{pmatrix} b_{11} & b_{12} \\ b_{21} & b_{22} \end{pmatrix}$$

is nonsingular and so can be inverted to obtain α_1 and α_2, the values of the incoming characteristics, as a function of α_3, the value of the outgoing characteristic.

Similarly the outflow boundary condition yields one equation of the form

$$C_{out} U = 0 \tag{18}$$

and substitution of (14) produces

$$\begin{pmatrix} b_{31} & b_{32} & b_{33} \end{pmatrix} \begin{pmatrix} \alpha_1 \\ \alpha_2 \\ \alpha_3 \end{pmatrix} = 0, \tag{19}$$

where

$$\begin{pmatrix} b_{31} & b_{32} & b_{33} \end{pmatrix} = C_{out} \begin{pmatrix} e^{i(\omega/\lambda_1)} U_1 & e^{i(\omega/\lambda_2)} U_2 & e^{i(\omega/\lambda_3)} U_3 \end{pmatrix}. \tag{20}$$

The second necessary condition for the wellposedness of the initial boundary value problem is that b_{33} is nonzero so that α_3 the value of the incoming characteristic can be determined as a function of α_1 and α_2 the values of the outgoing characteristics.

Equations (16) and (19) can be written jointly as

$$B(\omega) \begin{pmatrix} \alpha_1 \\ \alpha_2 \\ \alpha_3 \end{pmatrix} = 0. \tag{21}$$

To obtain a nontrivial eigenmode $B(\omega)$ must be singular and the vector $(\alpha_1 \quad \alpha_2 \quad \alpha_3)^T$ must be a corresponding null vector. Thus the eigenfrequenices can be calculated from the following determinant equation

$$\det B(\omega) = 0. \tag{22}$$

The matrix B can also be used to examine whether the steady-state boundary value problem is wellposed. The three requirements for wellposedness are that a solution exists, is unique, and small perturbations in the boundary data produce small perturbations in the solution.

The linearized steady-state boundary value problem has a zero solution and this solution is unique provided there are no nonzero solutions to

$$B(0)\begin{pmatrix}\alpha_1\\ \alpha_2\\ \alpha_3\end{pmatrix} = 0, \tag{23}$$

i.e., provided that B(0) is non-singular.

A perturbation of the boundary data leads to an equation of the form

$$B(0)\begin{pmatrix}\alpha_1\\ \alpha_2\\ \alpha_3\end{pmatrix} = \begin{pmatrix}\beta_1\\ \beta_2\\ \beta_3\end{pmatrix}, \tag{24}$$

which, provided B(0) is nonsingular, can be solved to obtain $(\alpha_1 \quad \alpha_2 \quad \alpha_3)^T$ which define the characteristic perturbations of the steady-state solution.

Thus the linearized steady-state boundary value problem is wellposed if, and only if, det B(0) is nonzero, or alternatively the initial boundary value problem does not have a zero eigenfrequency.

3. EXAMPLES

(a) Entropy, Enthalpy Specified at Inflow, Pressure at Outflow

The physical boundary conditions are

$$X = 0 \quad \begin{cases} p'/\rho'^{\gamma} = \bar{p}/\bar{\rho}^{\gamma} & (25a) \\ \frac{\gamma-1}{2} u'^2 + \frac{\gamma p'}{\rho'} = \frac{\gamma-1}{2} \bar{u}^2 + \frac{\gamma \bar{p}}{\bar{\rho}} & (25b) \end{cases}$$

$$X = L \qquad p' = \bar{p}, \qquad (25c)$$

where ρ', u', p' are the unsteady physical variables which are a sum of the steady-state and unsteady perturbation variables. The corresponding linearized non-dimensionalized equations are

$$x = 0 \quad \begin{pmatrix} -1 & 0 & 1 \\ & & \\ -1 & (\gamma-1)M & \gamma \end{pmatrix} \begin{pmatrix} \rho \\ u \\ p \end{pmatrix} = 0, \qquad (26a)$$

$$x = 1 \quad \begin{pmatrix} 0 & 0 & 1 \end{pmatrix} \begin{pmatrix} \rho \\ u \\ p \end{pmatrix} = 0. \qquad (26b)$$

At $x = 0$ substitution of the eigenvector definitions (11b), (12b), and (13b) into the eigenmode definition (14) yields

$$\begin{pmatrix} \rho \\ u \\ p \end{pmatrix} = e^{-i\omega t} \begin{pmatrix} 1 & 1 & 1 \\ 0 & 1 & -1 \\ 0 & 1 & 1 \end{pmatrix} \begin{pmatrix} \alpha_1 \\ \alpha_2 \\ \alpha_3 \end{pmatrix}. \qquad (27)$$

Substitution of this equation into (26a) produces the characteristic inflow boundary condition

$$\begin{pmatrix} -1 & 0 & 1 \\ -1 & (\gamma-1)M & \gamma \end{pmatrix} \begin{pmatrix} 1 & 1 & 1 \\ 0 & 1 & -1 \\ 0 & 1 & 1 \end{pmatrix} \begin{pmatrix} \alpha_1 \\ \alpha_2 \\ \alpha_3 \end{pmatrix}$$

$$= \begin{pmatrix} -1 & 0 & 0 \\ -1 & (\gamma-1)(1+M) & (\gamma-1)(1-M) \end{pmatrix} \begin{pmatrix} \alpha_1 \\ \alpha_2 \\ \alpha_3 \end{pmatrix} = 0. \qquad (28)$$

Similarly at $x = 1$

$$\begin{pmatrix} \rho \\ u \\ p \end{pmatrix} = e^{-i\omega t} \begin{pmatrix} 1 & 1 & 1 \\ 0 & 1 & -1 \\ 0 & 1 & 1 \end{pmatrix} \begin{pmatrix} \alpha_1 \exp(i\omega/\lambda_1) \\ \alpha_2 \exp(i\omega/\lambda_2) \\ \alpha_3 \exp(i\omega/\lambda_3) \end{pmatrix}, \qquad (29)$$

and substitution into (26b) produces the characteristic outflow boundary condition

$$(0 \quad 0 \quad 1) \begin{pmatrix} 1 & 1 & 1 \\ 0 & 1 & -1 \\ 0 & 1 & 1 \end{pmatrix} \begin{pmatrix} \alpha_1 \exp(i\omega/\lambda_1) \\ \alpha_2 \exp(i\omega/\lambda_2) \\ \alpha_3 \exp(i\omega/\lambda_3) \end{pmatrix}$$

$$= \begin{bmatrix} 0 & \exp(i\omega/\lambda_2) & \exp(i\omega/\lambda_3) \end{bmatrix} \begin{pmatrix} \alpha_1 \\ \alpha_2 \\ \alpha_3 \end{pmatrix} = 0 . \qquad (30)$$

Together equations (28) and (30) define the matrix B

$$B(\omega) = \begin{pmatrix} -1 & 0 & 0 \\ -1 & (\gamma-1)(1+M) & (\gamma-1)(1-M) \\ 0 & \exp(i\omega/\lambda_2) & \exp(i\omega/\lambda_3) \end{pmatrix} . \qquad (31)$$

The eigenfrequencies are given by

$$\det B = (\gamma-1)\left[(1-M)\exp(i\omega/\lambda_2) - (1+M)\exp(i\omega/\lambda_3)\right] = 0, \tag{32}$$

$$\Longrightarrow \exp\left(\frac{2i\omega}{1-M^2}\right) = \frac{1+M}{1-M}, \tag{33}$$

$$\Longrightarrow \omega = \frac{1-M^2}{2}\left[-i\log\left(\frac{1+M}{1-M}\right) + 2n\pi\right], \tag{34}$$

where n is an integer.

Thus there is an infinite set of discrete eigenfrequencies. It is useful to define a decay rate σ_n

$$\sigma_n \overset{\text{def}}{=} -\mathrm{Im}(\omega_n). \tag{35}$$

For this example

$$\sigma_n = \frac{1-M^2}{2}\log\left(\frac{1+M}{1-M}\right). \tag{36}$$

The amplitude of the eigenmode grows, or decays, as $\exp(-\sigma t)$, so the requirement for all eigenmodes to decay is $\sigma_n > 0$ for every n. In this example the requirement is satisfied and so any initial disturbance at $t = 0$ will decay exponentially.

(b) Mass Flux, Enthalpy Specified at Inflow, Pressure at Outflow

The physical boundary conditions are

$$X = 0 \quad \begin{cases} \rho' u' = \bar{\rho}\,\bar{u} & (37a) \\ \dfrac{\gamma-1}{2}u'^2 + \dfrac{\gamma p'}{\rho'} = \dfrac{\gamma-1}{2}\bar{u}^2 + \dfrac{\gamma\bar{p}}{\bar{\rho}} & (37b) \end{cases}$$

$$X = L \qquad p' = \bar{p}. \tag{37c}$$

Omitting the algebraic details the resultant matrix B is

$$B = \begin{pmatrix} M & 1+M & M-1 \\ -1 & (\gamma-1)(1+M) & (\gamma-1)(1-M) \\ 0 & \exp(i\omega/\lambda_2) & \exp(i\omega/\lambda_3) \end{pmatrix} . \tag{38}$$

The eigenfrequencies are

$$\omega_n = \frac{1-M^2}{2}\left[-i\log\left(\frac{(1+M)[1+M(\gamma-1)]}{(1-M)[1-M(\gamma-1)]}\right) + 2(n+\tfrac{1}{2})\pi\right] . \tag{39}$$

The decay rates are

$$\sigma_n = \frac{1-M^2}{2}\log\left(\frac{(1+M)[1+M(\gamma-1)]}{(1-M)[1-M(\gamma-1)]}\right) . \tag{40}$$

(c) Density, Pressure Specified at Inflow, Pressure at Outflow

The physical boundary conditions are

$$X = 0 \quad \begin{cases} \rho' = \bar{\rho} & (41a) \\ p' = \bar{p} & (41b) \end{cases}$$

$$X = L \qquad p' = \bar{p} . \tag{41c}$$

The matrix B is

$$B = \begin{pmatrix} 1 & 1 & 1 \\ 0 & 1 & 1 \\ 0 & \exp(i\omega/\lambda_2) & \exp(i\omega/\lambda_3) \end{pmatrix} . \tag{42}$$

The eigenfrequenices are

$$\omega_n = (1 - M^2)n\pi \ , \tag{43}$$

and the decay rates are zero.

Since one of the eigenfrequenices is zero the steady-state boundary value problem is ill-posed, as discussed earlier.

(d) Density, Velocity Specified at Inflow, Pressure at Outflow

The physical boundary conditions are

$$X = 0 \qquad \begin{cases} \rho' = \bar{\rho} & (44a) \\ u' = \bar{u} & (44b) \end{cases}$$

$$X = L \qquad p' = \bar{p}. \tag{44c}$$

The matrix B is

$$B = \begin{pmatrix} 1 & 1 & 1 \\ 0 & 1 & -1 \\ 0 & \exp(i\omega/\lambda_2) & \exp(i\omega/\lambda_3) \end{pmatrix} \ . \tag{45}$$

The eigenfrequenices are

$$\omega_n = (1 - M^2)(n + 1/2)\pi \tag{46}$$

and the decay rates are zero.

In this example the steady-state boundary value problem is wellposed but because of the zero decay rates unsteady oscillations will continue indefinitely without exponential growth or decay.

(e) Non-reflecting Boundary Conditions

The full nonlinear non-reflecting boundary conditions specify entropy and the appropriate Riemann invariant at the inflow, and the other Riemann invariant at the outflow [4]

$$X = 0 \quad \begin{cases} p'/\rho'^{\gamma} = \bar{p}/\bar{\rho}^{\gamma} & (47a) \\ u' + \frac{2}{\gamma-1} c' = \bar{u} + \frac{2}{\gamma-1} \bar{c} & (47b) \end{cases}$$

$$X = L \qquad u' - \frac{2}{\gamma-1} c' = \bar{u} - \frac{2}{\gamma-1} \bar{c} \; . \qquad (47c)$$

The matrix B is

$$B = \begin{pmatrix} -1 & 0 & 0 \\ -\frac{1}{\gamma-1} & 2 & 0 \\ \frac{1}{\gamma-1} \exp(i\omega/\lambda_1) & 0 & -2 \exp(i\omega/\lambda_3) \end{pmatrix} . \qquad (48)$$

Det B = 0 leads to $\sigma = +\infty$ which reflects the fact that with these boundary conditions the unsteady perturbations become zero after the finite time it takes for all three characteristic waves to cross the domain once.

CONCLUSIONS

The calculation of the exponential decay rates of physical eigenmodes has implications for the stability and convergence rates of time-marching finite difference computations. If the analytic problem has exponentially increasing eigenmodes then for sufficiently fine grid resolution a time-accurate numerical solution will exhibit corresponding exponentially increasing

eigenmodes. In a forthcoming paper, Trefethen [8] will prove that for a linear constant coefficient system such as this the three conditions:

(i) Exponentially decaying physical eigenmodes,

(ii) Dissipative interior numerical scheme,

(iii) GKS-stable numerical boundary conditions,

are sufficient to ensure the P-stability of a time-marching method for a sufficiently fine grid. P-stability was defined by Beam, Warming and Yee [2] and corresponds to GKS-stability with the additional requirement that none of the numerical eigenmodes increases exponentially. The precise definition of the theorem and its proof are given in [8], but in essence the argument is that condition (i) ensures that low frequency physical waves decay, while conditions (ii) and (iii) ensure the decay of high frequency waves, both physical and non-physical.

The exponential decay rates for the physical eigenmodes also provide a useful lower limit on the spectral radius of the finite difference time-marching procedure. If a physical eigenmode decays as $\exp(-\sigma t)$ with $\sigma > 0$, then for a sufficiently fine grid the corresponding numerical eigenmode decays approximately as $\exp(-\sigma\, n\, \Delta t)$ where n is the iteration number and Δt is the time-step. As the grid is refined with $\Delta t/\Delta x$ held constant, $\Delta t \to 0$ and so the spectral radius is no less than $1 - \sigma\Delta t + O(\Delta t^2)$. If $\sigma = 0$, as in example (d), the physical eigenmodes are neutrally stable and so the numerical convergence rate towards steady-state is due solely to numerical dissipation. If this dissipation is of n^{th} order then the corresponding spectral radius is $1 - O(\Delta t^{n+1})$. Non-reflecting boundary conditions as in example (e) clearly give a much faster rate of convergence, but in two or three dimensions perfectly non-reflecting boundary conditions do not exist and in general the best that can be achieved is that there is zero

reflection for locally plane waves propagating in a particular chosen direction [1].

It is not clear to what extent the conclusions for this model problem, with linearized perturbations and constant coefficients, are valid for more general flows such as transonic quasi-one-dimensional and two-dimensional flows. Nonlinear mechanisms at sonic lines and shocks are undoubtedly very important. However the decay to steady-state of low frequency waves will still depend on the physical boundary conditions and so this analysis should provide insight into the effect of the boundary conditions.

REFERENCES

[1] A. Bayliss and E. Turkel, "Radiation Boundary Conditions for Wave-Like Equations," Comm. Pure Appl. Math., Vol. 33, 1980, pp. 707-725.

[2] R. M. Beam, R. F. Warming, and H. C. Yee, "Stability Analysis of Numerical Boundary Conditions and Implicit Difference Approximations for Hyperbolic Equations," Numerical Boundary Condition Procedures, NASA CP-2201, 1981, pp. 257-282.

[3] M. Giles and W. T. Thompkins, Jr., "Asymptotic Analysis of Numerical Wave Propagation in Finite Difference Equations," Gas Turbine and Plasma Dynamics Laboratory Report 171, Massachusetts Institute of Technology, 1983.

[4] H.-O. Kreiss, "Initial Boundary Value Problems for Hyperbolic Systems," Comm. Pure Appl. Math., Vol. 23, 1970, pp. 277-298.

[5] J. Lighthill, Waves in Fluids, Cambridge University Press, 1978, pp. 137-152.

[6] P. M. Morse and K. U. Ingard, Theoretical Acoustics, International Series in Pure and Applied Physics, McGraw-Hill, 1968.

[7] J. Oliger and A. Sundström, "Theoretical and Practical Aspects of Some Initial Boundary Value Problems in Fluid Dynamics," SIAM, Vol. 25, No. 3, 1978, pp. 419-446.

[8] L. N. Trefethen, "Stability of Finite Difference Models Containing Two Boundaries or Interfaces," to appear.

[9] S. F. Wornom and M. M. Hafez, "A Rule for Selecting Analytical Boundary Conditions for the Conservative Quasi-One-Dimensional Nozzle Flow Equations," in AIAA 22nd Aerospace Sciences Meeting, January 1984.

SOLUTION OF 1-D EULER EQUATIONS USING A BOX METHOD

M. Giles

CFDL-TR-84-1 February 1984

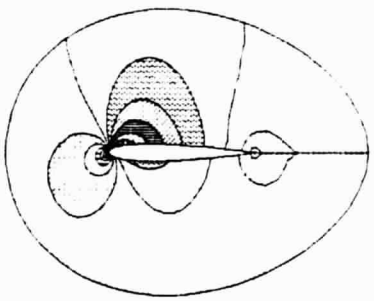

COMPUTATIONAL FLUID DYNAMICS LABORATORY

Department of Aeronautics and Astronautics

Massachusetts Institute of Technology

Cambridge, Massachusetts 02139

SOLUTION OF 1-D EULER EQUATIONS USING A BOX METHOD

M. Giles

CFDL-TR-84-1 February 1984

This work was supported by
NASA Grant No. NAG3-9,
supervised by Dr. R. V. Chima.

Department of Aeronautics and Astronautics
Massachusetts Institute of Technology
Cambridge, Massachusetts 02139

Abstract

The unsteady quasi-one-dimensional Euler equations are solved using a conservative box method which is second order accurate and requires no non-physical boundary conditions. No artificial viscosity is used and so the shock cells and sonic cells require special treatment which is related to the behavior of the analytic characteristics. Results are given for a converging-diverging channel with a moving shock due to the periodic oscillation of the inlet boundary conditions.

Notation

Variables

A	Cross-sectional area of duct
c	Speed of sound
E	Enthalpy
F	Flux vector
p	Pressure
P	Pressure vector
u	Velocity
U	Conservative state vector
ρ	Density
γ	Ratio of specific heats

Subscripts

j	Spatial index for discrete variables
^{0}	Stagnation quantity
e	Exit quantity

Superscript

n	Iteration number for discrete variables

1. Introduction

The box method was first proposed by Keller [1] for solving parabolic equations in which the second order p.d.e. is first rewritten as a coupled system of first order p.d.e.'s. It is now widely used for solving the boundary layer equations. It also has several attractive features for solving hyperbolic systems. It is second order accurate, requires no non-physical boundary conditions (such as extrapolation of characteristics as required by 3-point differencing schemes) and for the model problem $u_t+cu_x = 0$ it gives the exact answer if $c\Delta t/\Delta x=1$.

The box method was first used to solve the 1-D Euler equations by S. Wornom [2]. Since Wornom was interested in steady-state solutions he used a Backward Euler version of the box method and assumed constant stagnation enthalpy. For large Δt this converges rapidly to the steady state solution. In supersonic regions artificial compressibilty was introduced (as proposed by Eberle [4]) to achieve shock capturing and prevent expansion shocks near the sonic point. As a consequence one non-physical boundary condition was required at the supersonic outlet and this produced a boundary-layer type behavior at the outlet. Wornom has also used the time-accurate box method to solve the 1-D unsteady Euler equations [3]. In this paper he chose not to use artificial compressibilty and consequently did not require any non-physical boundary conditions but did require special treatment of the sonic cell and was unable to handle the shock cell.

In section 2 of this report the conservative equations are derived for subsonic cells (cells for which both the inflow and the outflow are subsonic), and supersonic cells (cells for which both the inflow and the outflow are supersonic). These equations are identical to those used by Wornom [3]. Section 3 derives the physical boundary conditions and their numerical implementation. Section 4 discusses the difficulties with sonic cells (cells for which the inflow is subsonic but the outflow is supersonic), and shock cells (cells for which the

inflow is supersonic but the outflow is subsonic), and their relation to the behavior of the analytic charcteristics. For the sonic cell the difficulties are resolved by imposing an additional characteristic equation. For the shock cell a natural form of shock fitting is derived with the shock position being an additional variable. Section 5 presents a computational example of a convergent-divergent channel with a shock which oscillates due to a periodic oscillation in the inlet stagnation pressure. Finally section 6 discusses the results and the difficulties and current achievements in extensions to the two-dimensional Euler equations.

2. Equations for Subsonic and Supersonic Cells

The unsteady quasi-one-dimensional Euler equations for a variable area nozzle are,

$$\frac{\partial}{\partial t}(AU) + \frac{\partial}{\partial x}(AF) + A\frac{\partial P}{\partial x} = 0 \tag{1}$$

where

$$U = \begin{pmatrix} \rho \\ \rho u \\ \rho E \end{pmatrix} \qquad F = \begin{pmatrix} \rho u \\ \rho u^2 \\ (\rho E+p)u \end{pmatrix} \qquad P = \begin{pmatrix} 0 \\ p \\ 0 \end{pmatrix} \tag{2-4}$$

An integral form of Eq. (1) for any computational cell is,

$$\frac{\partial}{\partial t}\int_{x_j}^{x_{j+1}} AU\,dx + AF\Big|_{x_j}^{x_{j+1}} + \int_{x_j}^{x_{j+1}} A\frac{\partial P}{\partial x}\,dx = 0 \tag{5}$$

This equation remains valid even when there is a shock in the interval $[x_j, x_{j+1}]$ (provided $\frac{\partial P}{\partial x}$ is correctly represented by a Dirac delta function) and is the basis of the finite difference equations.

As illustrated in figure 1 the approximations which are introduced are that A is piecewise linear between x_j and x_{j+1} and U is piecewise constant between $x_{j-\frac{1}{2}}$ and $x_{j+\frac{1}{2}}$. With these approximations eq.(5) becomes,

$$(x_{j+1}-x_j)\frac{\partial}{\partial t}\left(\frac{1}{2}A_{j+\frac{1}{2}}U_j + \frac{1}{2}A_{j+\frac{1}{2}}U_{j+1}\right) + A_{j+1}F_{j+1} - A_jF_j + A_{j+\frac{1}{2}}(P_{j+1}-P_j) = 0 \tag{6}$$

where $A_{j+\Delta j}=A_j+\Delta j(A_{j+1}-A_j)$. Now $\frac{\partial}{\partial t}U_j$ is approximated by $\frac{1}{\Delta t}(U_j^{n+1}-U_j^n)$ and the flux term F_j (and similarly P_j) is approximated at time level $n+\theta$ by a linearized expansion $F_j^{n+\theta}=F_j^n+\theta\frac{\partial F}{\partial U}(U_j^{n+1}-U_j^n)$. $\theta=1$ corresponds to the Backward Euler version while $\theta=1/2$ corresponds to the time-accurate box scheme used by Wornom in [3]. Thus the finite difference equations which are used are,

$$\frac{\Delta x}{\Delta t}\left(\frac{1}{2}A_{j+\frac{1}{2}}\,\Delta U_j^n+\frac{1}{2}A_{j+\frac{1}{2}}\,\Delta U_{j+1}^n\right)+$$
$$+\;A_{j+1}\left(F_{j+1}^n+\theta\frac{\partial F}{\partial U}\Delta U_{j+1}^n\right)-A_j\left(F_j^n+\theta\frac{\partial F}{\partial U}\Delta U_j^n\right)$$
$$+\;A_{j+\frac{1}{2}}\left(P_{j+1}^n+\theta\frac{\partial P}{\partial U}\Delta U_{j+1}^n-P_j^n-\theta\frac{\partial P}{\partial U}\Delta U_j^n\right)=0 \qquad (7)$$

In matrix form the equations are,

$$B_j^n\,\Delta U_j^n+C_j^n\,\Delta U_{j+1}^n=-R_{j+\frac{1}{2}}^n \qquad (8)$$

where,

$$B_j^n=\frac{\Delta x}{2\Delta t}A_{j+\frac{1}{2}}\,I-\theta A_j\frac{\partial F}{\partial U}-\theta A_{j+\frac{1}{2}}\frac{\partial P}{\partial U} \qquad (9)$$

$$C_j^n=\frac{\Delta x}{2\Delta t}A_{j+\frac{1}{2}}\,I+\theta A_{j+1}\frac{\partial F}{\partial U}+\theta A_{j+\frac{1}{2}}\frac{\partial P}{\partial U} \qquad (10)$$

$$R_{j+\frac{1}{2}}=\begin{pmatrix} A_{j+1}(\rho u)_{j+1}^n-A_j(\rho u)_j^u \\ A_{j+1}(\rho u^2)_{j+1}^n-A_j^n(\rho u^2)_j^n+A_{j+\frac{1}{2}}(p_{j+1}^n-p_j^n) \\ A_{j+1}(\rho E+p)u_{j+1}^n-A_j(\rho E+p)u_j^n \end{pmatrix} \qquad (11)$$

$$\frac{\partial F}{\partial U}=\begin{pmatrix} 0 & 1 & 0 \\ -u^2 & 2u & 0 \\ -\gamma Eu+(\gamma-1)u^3 & \gamma E-\frac{3}{2}(\gamma-1)u^2 & \gamma \end{pmatrix} \qquad (12)$$

$$\frac{\partial P}{\partial U} = \begin{pmatrix} 0 & 0 & 0 \\ \frac{1}{2}(\gamma-1)u^2 & -(\gamma-1)u & \gamma-1 \\ 0 & 0 & 0 \end{pmatrix} \tag{13}$$

3. Boundary Conditions

a) Supersonic Inlet and Outlet

At supersonic inlets there are three boundary conditions which together totally specify the flow variables at the inlet. At supersonic outlets there are no physical boundary conditions, and no boundary conditions are required for the numerical solution.

b) Subsonic Inlet

At subsonic inlets two boundary conditons are required and they are chosen to be specified stagnation pressure and density. For programming simplicity these are implemented through the following equivalent two conditions.

$$\left(p\ \rho^{-\gamma}\right)_1^{n+1} = p_0\ \rho_0^{-\gamma} \tag{14}$$

which when linearized becomes,

$$\left(\frac{\gamma-1}{2}\ u^2-c^2\right)_1^n \Delta\rho_1^n - (\gamma-1)u_1\ \Delta(\rho u)_1^n + (\gamma-1)\ \Delta(\rho E)_1^n = -P_1^n + p_0(\rho_1^n/\rho_0)^\gamma \tag{15}$$

and

$$\left(\frac{\gamma-1}{2}\ u^2 + c^2\right)_1^{n+1} = c_0^2 \tag{16}$$

which when linearized becomes,

$$\left(\frac{(\gamma-1)^2}{2}u^2 - c_0^2\right)_1^n \Delta\rho_1^n - (\gamma-1)^2 u_1^n\ \Delta(\rho u)_1^n + \gamma(\gamma-1)\ \Delta(\rho E)_1^n = -\rho_1^n\left(\frac{\gamma-1}{2}\ u^2 + c^2 - c_0^2\right)_1^n \tag{17}$$

c) Subsonic Outlet

At subsonic outlets one boundary condition is required which is chosen to be specified exit pressure.

$$p_J^{n+1} = p_e \tag{18}$$

which when linearized becomes,

$$\left(\frac{\gamma-1}{2} u^2\right)_J^n \Delta\rho_J^n - (\gamma-1)u_J^n \Delta(\rho u)_J^n + (\gamma-1) \Delta(\rho E)_J^n = p_e - p_J^n \tag{19}$$

4. Equations for Sonic and Shock Cells

In a case in which the flow is supersonic in the entire domain, the inlet flow is specified and the matrix equation (7) can be solved to obtain ΔU_2 and then the other ΔU_j by marching downstream. In a case in which the flow is subsonic in the entire domain, there are 3J variables, (the ΔU at $1<j<J$), 3(J-1) cell equations and 3 boundary conditions, two at the inlet and one at the outlet. Thus the number of equations equals the number of variables. The system can be written as a block tridiagonal set of equations with 3x3 blocks and solved by standard methods. If $\theta=0.5$ the equations reduce in both cases to those used by Wornom [3].

Solutions for the above two flow problems are straightforward. The difficulties arise with shocks and sonic points. Consider the case in which the flow is supersonic at the inlet and subsonic at the outlet. There are still 3J flow variables and 3(J-1) cell equations, but now there are 4 boundary conditions so there is one more equation than variable. This can be understood by considering the behavior of the analytic characteristics. The characteristic velocities are u,u±c so there are four characteristics entering the shock cell, three on the supersonic inflow side of the cell and one on the subsonic outflow side. For a steady-state problem the "characteristic information" from the u-c characteristics entering the cell on each side must match, but in an unsteady problem the mismatch determines the shock velocity. This suggests that some form of shock fitting is neccessary. The procedure chosen was to define one additional variable, x_s, the shock position. In the shock cell it is assumed that,

$$U = \begin{cases} U_j & x_j < x < x_s \\ U_{j+1} & x_s < x < x_{j+1} \end{cases} \tag{20}$$

as illustated in figure 2, and so defining λ^n by

$$x_s(t_n) = x_j + \lambda^n (x_{j+1} - x_j) \tag{21}$$

the conservation equation with spatial discretization is,

$$(x_{j+1}-x_j)\frac{\partial}{\partial t}\left(\frac{1}{2} A_{j+\lambda/2} U_j + \frac{1}{2} A_{j+(1+\lambda)/2} U_{j+1}\right) + A_{j+1} F_{j+1} - A_j F_j + A_{j+\lambda} (P_{j+1}-P_j) = 0 \tag{22}$$

and the fully discretized finite difference equation is,

$$\frac{\Delta x}{\Delta t}\left(\lambda^n A_{j+\lambda/2} \Delta U_j^n + (1-\lambda^n) A_{j+(1+\lambda)/2} \Delta U_{j+1}^n + A_{j+\lambda} (U_j^n - U_{j+1}^n) \Delta\lambda^n\right)$$
$$+ A_{j+1}\left(F_{j+1}^n + \theta \frac{\partial F}{\partial U} \Delta U_{j+1}^n\right) - A_j \left(F_j^n + \theta \frac{\partial F}{\partial U} \Delta U_j^n\right)$$
$$+ A_{j+\lambda}\left(P_{j+1}^n + \theta \frac{\partial P}{\partial U} \Delta U_{j+1}^n - P_j^n - \theta \frac{\partial P}{\partial U} \Delta U_j^n\right) + \theta (P_{j+1}^n - P_j^n) \frac{\partial A}{\partial j} \Delta\lambda^n = 0 \tag{23}$$

Note the two terms involving $\Delta\lambda^n$, the movement in the shock position. The first comes from the contribution to

$$\frac{\partial}{\partial t} \int_{x_j}^{x_{j+1}} AU \, dx$$

due to the movement of the shock, and the other is because the pressure jump acts across the shock area which changes in size when the shock moves.

Now that the number of variables equals the number of equations the system is well-posed and can be solved. If the shock moves upstream past the supersonic node, U at the supersonic node is replaced by U at the subsonic node. If the shock moves downstream past the subsonic node the opposite is done. One feature of this procedure is that it correctly calculates the velocity of a uniform moving shock in a constant area duct. Another is that in steady-state solutions the error in the shock position is $O(\Delta x^2)$ and so the global second order accuracy of the box scheme is preserved by this shock treatment.

In the case in which the flow is subsonic at the inlet, becomes sonic at a throat and is supersonic at the outlet, there are 3J variables, 3(J-1) cell equations and 2 boundary conditions. Thus there are one too few equations. An explanation of this is that at the sonic line two characteristics emerge with characteristic velocity u-c, one travelling upstream and one travelling downstream. In the Navier-Stokes equations the value propagated along these two characteristics would be determined by viscous forces in the neighborhood of the sonic point, but in the inviscid Euler equations an extra equation is required to set the characteristic value at the sonic point. By diagonalizing the Euler equations it can be shown [6] that the equation satisfied at the sonic point by the characteristic variable J_- with characteristic velocity $u-c=0$ is

$$\frac{\partial J_-}{\partial t} \equiv \frac{\partial p}{\partial t} - cu \frac{\partial u}{\partial t} = 0 \tag{24}$$

Thus the numerical condition which is imposed is that $\Delta J_-=0$ on the subsonic side of the sonic cell. When expressed in terms of conservation variables this becomes,

$$\left(\frac{\gamma+1}{2} u^2\right)_j^n \Delta\rho_j^n - \gamma u_j^n \Delta(\rho u)_j^n + (\gamma-1) \Delta(\rho E)_j^n = 0 \tag{25}$$

One other problem was found in actual computations near sonic points. A negative shock from subsonic to supersonic flow is a valid solution of the steady state Euler equations, and in practice small negative shocks often occurred. According to an inviscid isentropic analysis using Riemann invariants [5] these negative shocks should be unstable to small perturbations and should become expansion fans. Therefore the problem was solved by identifying negative shocks at the sonic point, and when they occurred smoothing the two points on either side of the shock. The shock then turned into an expansion fan and quickly the solution at the throat became an almost linear expansion from subsonic to supersonic flow.

5. Example

The test example is the unsteady problem of the flow through a choked converging-diverging nozzle with subsonic inflow and outflow, constant exit pressure and stagnation entropy and oscillating stagnation pressure. The nozzle area was defined by,

$$\frac{A(x)}{A^*} = 1. + (x-0.5)^2 \tag{26}$$

with $0<x<1$. 50 node points were used with x_j defined by,

$$x_j = \left(\frac{j-1}{49}\right) + \left(\left(\frac{j-1}{49}\right) - \frac{1}{2}\right)\left(\frac{1}{4} - \left(\left(\frac{j-1}{49}\right) - \frac{1}{2}\right)^2\right) \tag{27}$$

which gives slightly greater resolution near the throat. The stagnation pressure was defined by,

$$p_0 = \frac{1}{2}\,(p_{max}+p_{min}) + \frac{1}{2}\,(p_{max}-p_{min})\,\cos\left(\frac{2\pi n}{200}\right) \tag{28}$$

with,

$$p_{max}/p_{exit} = 1.4 \qquad p_{min}/p_{exit} = 1.2 \tag{29,30}$$

For reference steady flow is choked for $p_0/p_{exit} > 1.235$, and figures 3,4 show the steady-state solutions corresponding to p_{min} and p_{max} with the former being unchoked and the latter choked. Figure 5 shows the unsteady solution which remains choked at all times. The throat remains close to sonic throughout the oscillation and so there is little oscillation in Mach number between the inlet and the shock. The shock position varies greatly and so the outflow Mach number oscillates considerably. One interesting feature is the "wiggles" in the solution near the sonic line. The spatial wavelength of the induced oscillations is proportional to the local characteristic velocity. Near the sonic line u-c is small, so the wavelength of oscillations of the corresponding characteristic is small.

This problem has a time-step stability limit of approximately, $u_s\Delta t/\Delta x<0.2$ where u_s is the shock speed. The instability occurs when the shock is moving downstream. On the subsonic side of the shock cell U is defined to be constant in $x_s<x<x_{j+\frac{1}{2}}$. In the worst case $x_s^n = x_j$ and so if $\Delta x_s^n>(x_{j+1}-x_j)/2$ then j^{+1} is constant on a negative length. This justifies a stability limit of $u_s\Delta t/\Delta x<0.5$. In practice the block inversion in the subsonic solver becomes nearly singular at a lower Δt.

6. Conclusions

The most important conclusion is that it is possible to solve the Euler equations using a truly inviscid numerical method with no artificial viscosity and no spurious numerical boundary conditions. However this requires shock tracking and special treatment at sonic points to replace viscous mechanisms with appropriate inviscid conditions. In 1-D it is relatively easy to produce an efficient time-accurate scheme, but in 2-D the problems are much greater. In [3] Wornom develops a numerical scheme for steady-state two-dimensional Euler flow and presents an example of a supersonic shock reflection problem. Unfortunately the method is severely limited by a requirement that each of the characteristic velocities $u, u\pm c, v, v\pm c$ must not change in sign in the domain. In [7] Drela and Giles also develop methods for steady-state two-dimensional Euler flow using a conservative streamtube formulation. In supersonic applications the solution can be marched downstream, and accurately captures shocks without the introduction of artificial viscosity. In subsonic applications a very efficient relaxation procedure, similar to potential solvers, is used. In transonic applications artificial compressibility (very similar to that in [2]) is used to capture shocks. Further work is being done to improve the performance of the transonic solver. One possibility is a special treatment of sonic and shock cells in a manner analogous to that used in this paper. However at present no procedure for doing this has been found and, looking further ahead to 3-D calculations, it seems probable that a shock-capturing scheme will be much easier.

References

1 Keller, H.B.: A New Difference Scheme for Parabolic Problems. Numerical Solution of Partial Differential Equations, II, B. Hubbard ed. , Academic Press, Inc., 1971, pp.327-350

2 Wornom S.F.: Application of Two-Point Difference Schemes to the Conservative Euler Equations for One-Dimensional Flows, NASA Technical Memorandum No. 82262

3 Wornom, S.F.: Implicit Conservative Characteristic Modeling Schemes for Euler Equations - A New Approach, AIAA Paper 83-1939-CP, presented at 6th AIAA CFD Conference, July 13-15, 1983

4 Eberle, A.: A Method of Finite Volumes for the Calculation of Transonic Potential Flow About Wings Using the Minimum Pressure Integral, translation of MBB-Report UFE 1407(0), February 1978

5 Whitham, G.B.: Linear and Nonlinear Waves, pp 161-166, Wiley-Interscience, 1974

6 Yee, H.C., Beam, R.M. and Warming, R.F.: Stable Boundary Approximations for a Class of Implicit Schemes for the One-dimensional Inviscid Equations of Gas Dynamics, AIAA Paper 81-1009, Proceedings of AIAA 5th CFD Conference, June 1981

7 Drela, M. and Giles, M.: Conservative Streamtube Solution of Steady-State Euler Equations, MIT Dept. of Aero. and Astro. Report No. CFDL-TR-83-6, 1983

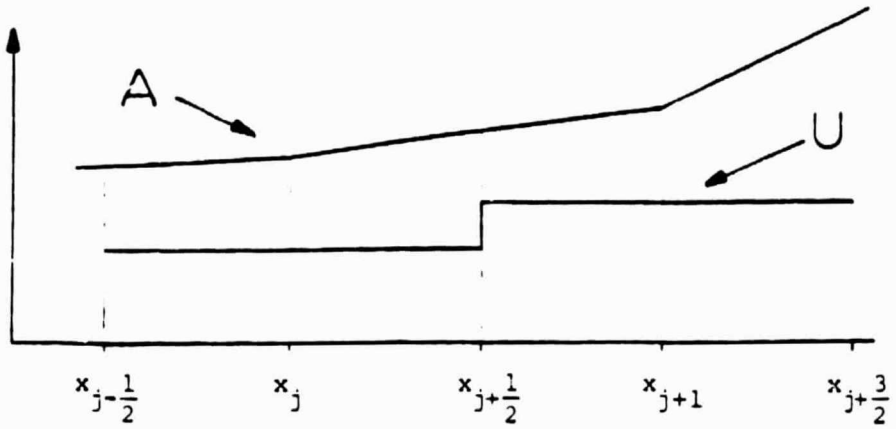

Figure 1. Illustration of piecewise linear definition of A and piecewise constant definition of U.

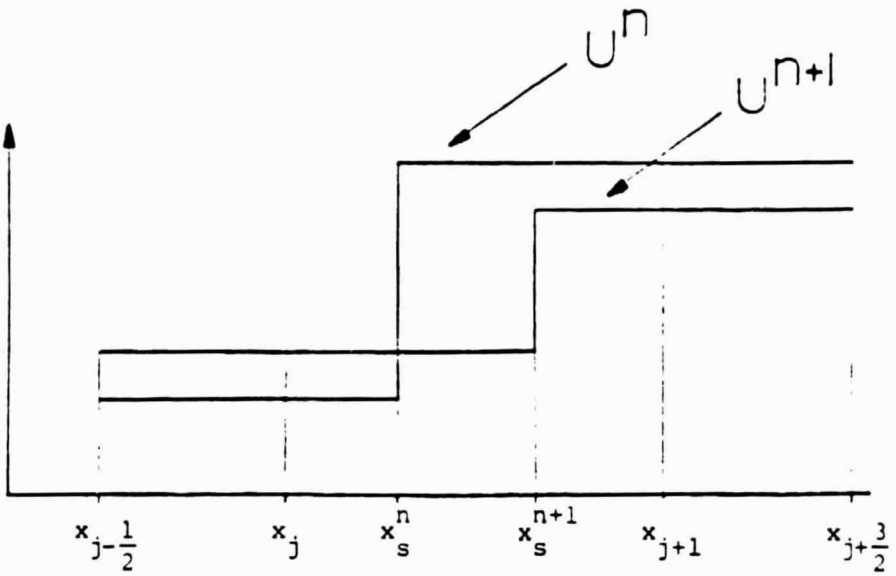

Figure 2. Illustration of piecewise constant definition of U in a shock cell with shock movement.

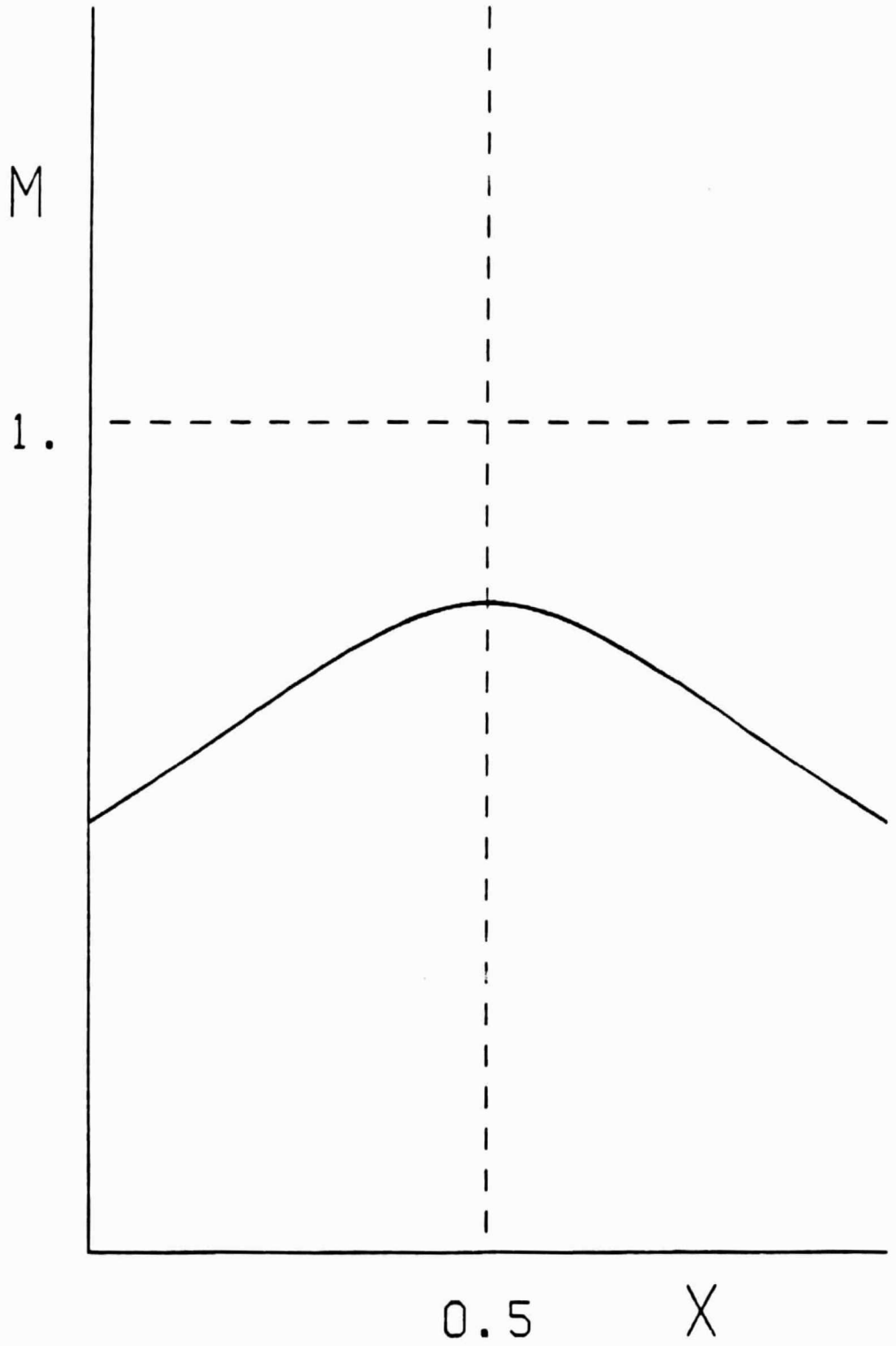

Figure 3. Mach number for steady-state solution with $p_o = p_{min}$

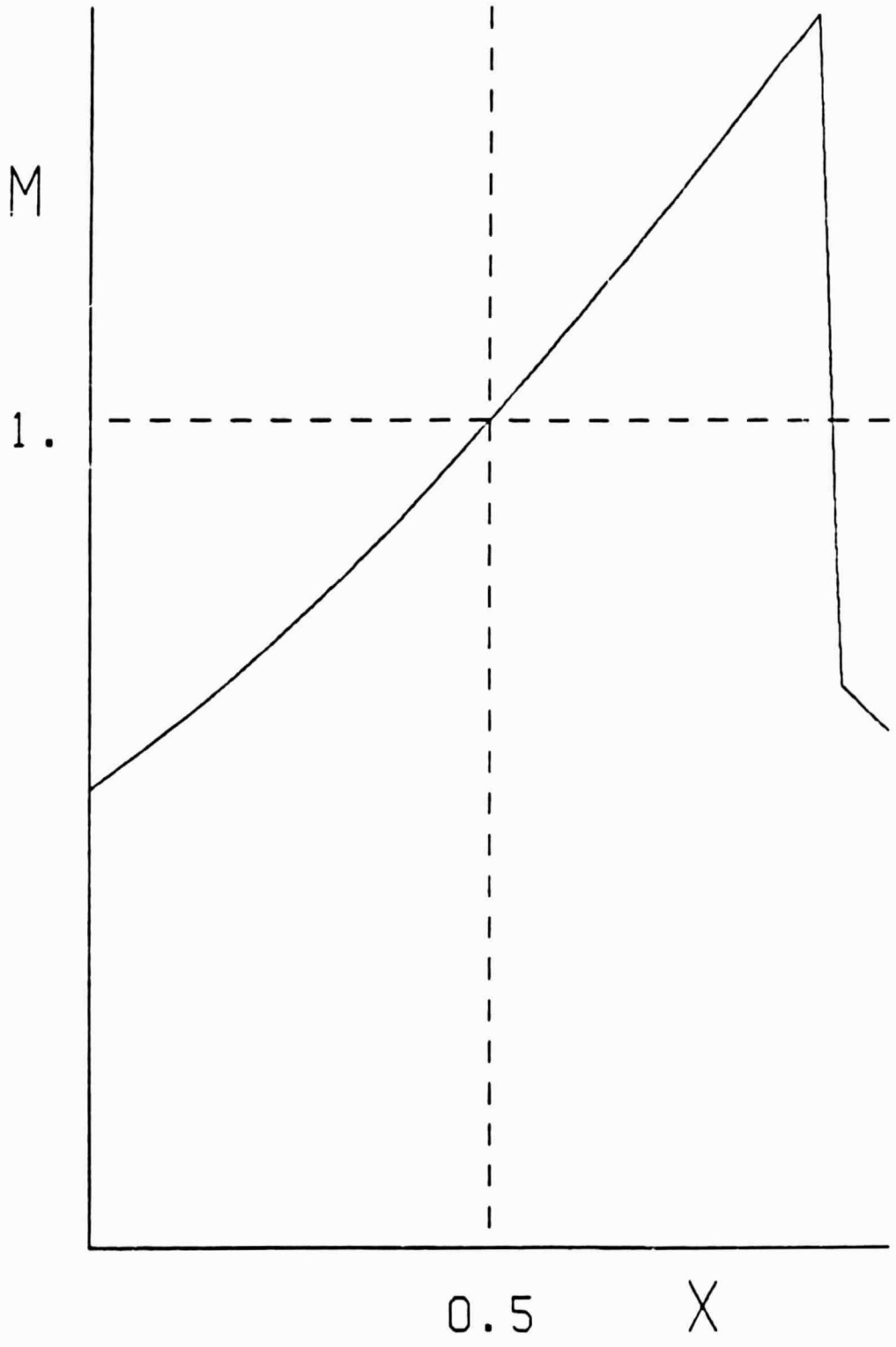

Figure 4. Mach number for steady-state solution with $p_o = p_{max}$

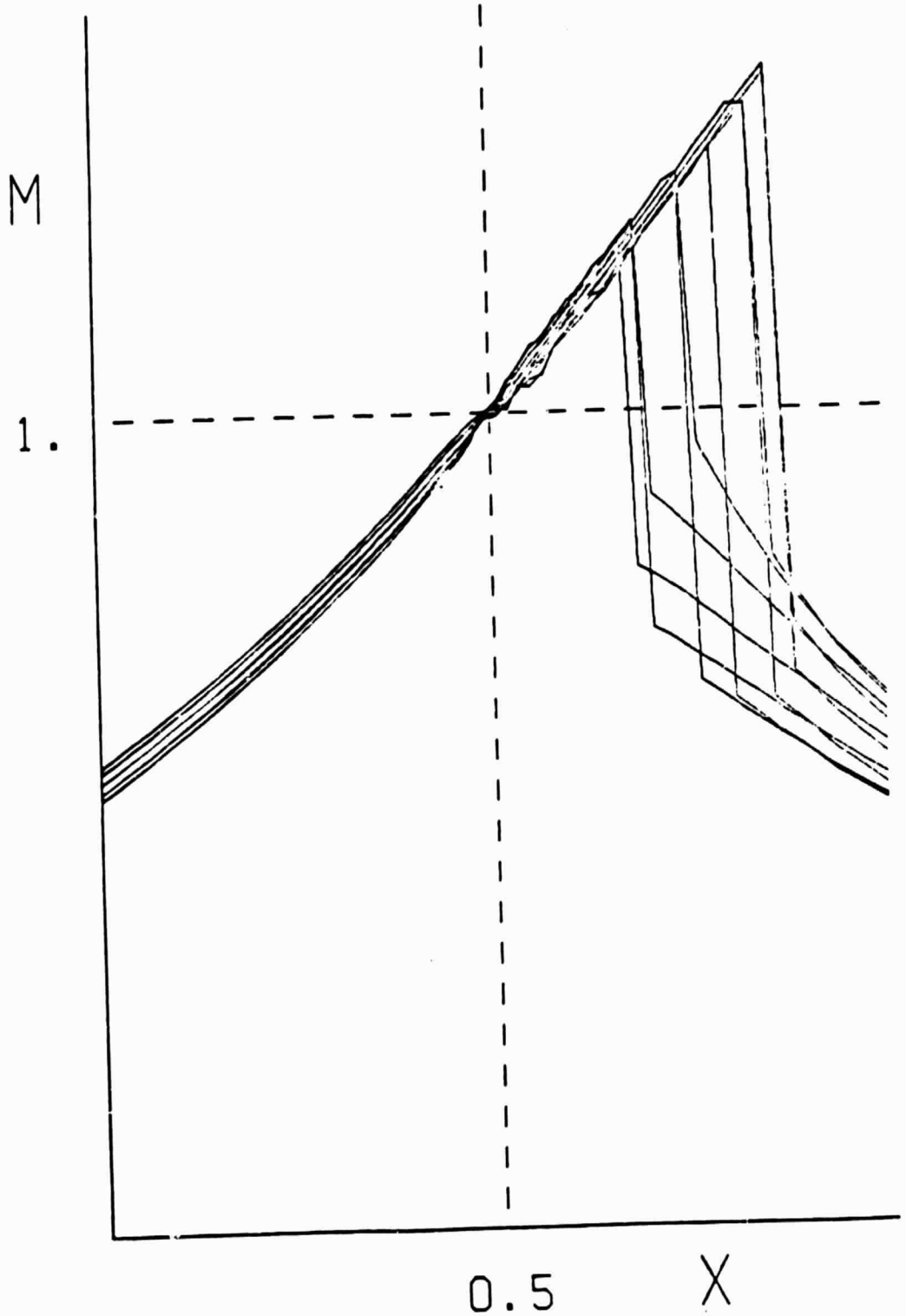

Figure 5. Mach number at equal intervals during oscillation of inlet stagnation pressure